The Pennsylvania State University

The Graduate School

Engineering Science and Mechanics Department

EXCITATION OF MULTIPLE SURFACE-PLASMON-POLARITON WAVES AT METAL/CHIRAL-SCULPTURED-THIN-FILM INTERFACES

A Thesis in

Engineering Science

by

Sema Erten

Submitted in Partial Fulfillment
of the Requirements
for the Degree of

Master of Science

August 2011

The thesis of Sema Erten was reviewed and approved* by the following:

Akhlesh Lakhtakia
The Charles G. Binder (Endowed) Professor of Engineering Science and Mechanics
Thesis Adviser

Osama O. Awadelkarim
Professor of Engineering Science and Mechanics

Judith A. Todd
P. B. Breneman Department Head Chair
Head of the Department of Engineering Science and Mechanics

*Signatures are on file in the Graduate School

Abstract

The objective of this research was to excite multiple surface-plasmon-polariton (SPP) waves guided by the interface of a metal and a chiral sculptured thin film (STF). For this purpose, three different experimental set-ups were used. The data were collected for several different samples. Aluminum, magnesium fluoride, zinc selenide and sodium fluoride are the materials that were used to deposit thin films.

Both metal and chiral STFs were deposited by a thermal evaporation technique. In all cases, a 30-nm-thick aluminum film was deposited first on a pre-cleaned glass slide. Next, to deposit a chiral STF, the substrate holder in the vacuum chamber of the thermal evaporation system was tilted and rotated. The vapor flux angle, i.e., the angle between incoming vapor flux and the substrate plane, is called χ_v. Chiral STFs deposited at $\chi_v = 10°$ and $\chi_v = 15°$ were used to understand the effects of different directions of the incoming vapor flux. Also, the thicknesses of chiral STFs were varied between 900 nm and 1500 nm. The chiral STFs were deposited in 3, 4, and 5 periods, each period being 300 nm in thickness. Besides chiral STFs, columnar thin films were deposited for comparison.

A He-Ne laser was used as a light source to illuminate the sample which was affixed to a BK7 glass prism, and the reflectance was detected by a photomultiplier detector for both p- and s- polarizations of the incident light. Graphs of the reflectance versus the angle of incidence were plotted.

If the angular location of a reflectance minimum is independent of the thickness of the chiral STF, then it is evidence of an SPP wave. Results of the experiments for Glass-slide/Aluminum/NaF-chiral-STF structure showed several reflectance minimums independent of the thickness of the chiral STF; hence, multiple SPP waves were launched. If more than one SPP wave can be launched guided by the interface of a metal and a thin film, this property can be used for many different applications including bio-chemical sensing.

Table of Contents

List of Figures

List of Tables

Acknowledgements

I thank my advisor, Dr. Akhlesh Lakhtakia for his continued support and encouragement throughout this research.

I thank Dr. Osama O. Awadelkarim for his help as a committee member for my defense and thesis.

I thank Drew P. Pulsifer and Muhammad Faryad for their help throughout this research.

I thank my family, Ayşe, Özden, and Özge Erten, for all their support over all these years.

Finally, I am grateful to the Turkish Republic Ministry of National Education for a scholarship to enable my studies at the Pennsylvania State University and also to the Charles Godfrey Binder Endowment at Penn State for partial financial support.

CHAPTER 1

Introduction

The aim of this study is to excite multiple surface-plasmon-polariton (SPP) waves guided by the interface of a metal and a periodically nonhomogeneous sculptured thin film (STF) at an optical frequency.

The quantum of plasma oscillations in a metal is called a plasmon. Surface plasmons propagate guided by the interface of a metal and vacuum. When the vacuum is replaced by a dielectric material, the quantum is called a surface plasmon-polariton, having a plasmonic component in the metal and a polaritonic component in the dielectric material. Energy exchange occurs between the two components continually, so that the excitation of a train of SPPs is often considered to be a resonant macroscopic phenomenon called surface plasmon resonance (SPR).

The classical analog of a train of SPPs is an SPP wave. SPP waves are usually excited optically. Monochromatic light is made to be incident at the metal-dielectric interface with a specific wave number parallel to the interface. The incident light must be p-polarized, i.e., the magnetic field vector must be oriented normal to the plane of incidence. Only one SPP wave, that too of the p-polarization state, can be excited at a given frequency, the dielectric material being isotropic and homogeneous [1]. The *sine qua non* for SPP waves is that the two partnering materials must have relative permittivities whose real parts differ in sign [2].

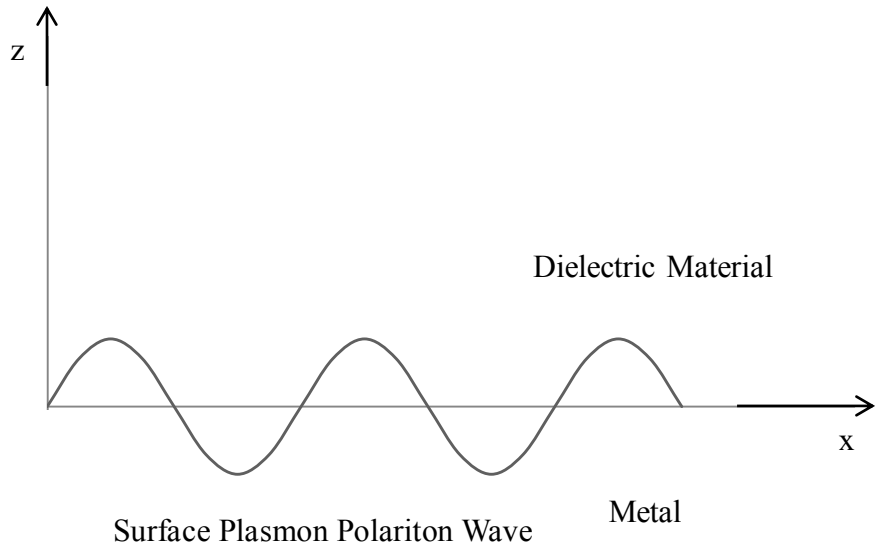

Figure 1.1 Schematic of an SPP wave guided by the interface of a metal and a dielectric material [2].

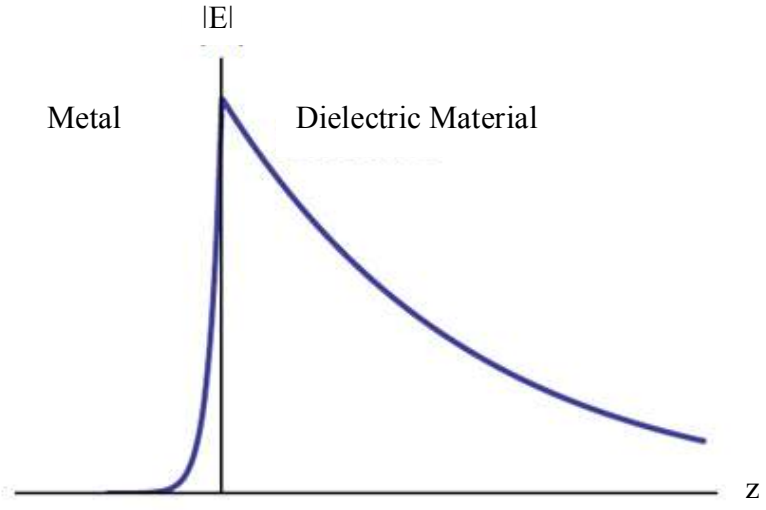

Figure 1.2 Typical profile of the magnitude of the electric field of a p-polarized SPP wave guided by the interface of a metal and an isotropic, homogeneous, dielectric material [2].

But, theoretical studies have proven that more than one SPP wave can be excited for both p-polarization (the direction of the electric field is wholly in the plane of incidence) and s-polarization (the direction of the electric field is perpendicular to the plane of incidence) of the incident light [2-4]. For this purpose, a periodically nonhomogeneous dielectric material should be used instead of the homogeneous dielectric material, the nonhomogeneity being in the direction normal to the interface. Also, experimental results have proven the excitation of multiple SPP waves at the interface of a metal and a periodically nonhomogeneous sculptured thin film [5-7].

1.1 Sculptured Thin Films (STFs)

A sculptured thin film is an assembly of parallel nanowires whose shape is engineered during the growth. Sculptured thin films are grown by physical vapor deposition typically, and can be fabricated from any material that can be evaporated. Dielectrics, metals and polymers are examples of the materials used to fabricate sculptured thin films [8]. The performance characteristics of STFs can be engineered by controlling the nanowire shape and constituent materials [8].

STFs are modifications of columnar thin films (CTFs) [9]. A CTF is deposited — generally by physical vapor deposition methods such as thermal evaporation, sputtering, and bombardment-enhanced evaporation — on a planar substrate located obliquely with respect to incoming vapor flux of the evaporated source material. The arriving adatoms settle and initially form nucleation clusters on the substrate. Due to self-shadowing effects, an array of tilted or upright columns grows. The columnar growth direction can be

changed continuously during growth to engineer the shape, leading to the formation of an STF. Any STF is porous and its voids define its morphology. A wide variety of columnar morphologies are possible by controlling the substrate rotation and rocking.

STFs can be morphologically classified as [10]:

(i) two-dimensional, sculptured nematic thin films (SNTFs) (e.g., simple slanted columns, chevrons, zigzags [11] or complex C-shapes and S-shapes [12]);

(ii) three-dimensional, thin film helicoidal bianisotropic mediums (TFHBMs) (e.g., simple helixes and super helixes [9,12]); and

(iii) combinations of two- and three-dimensional forms [13].

Chiral STFs are the commonest TFHBMs. Scanning electron microscope (SEM) images of chiral STFs, TFBMs and sculptured nematic thin films are shown in Figures 1.3 to 1.6.

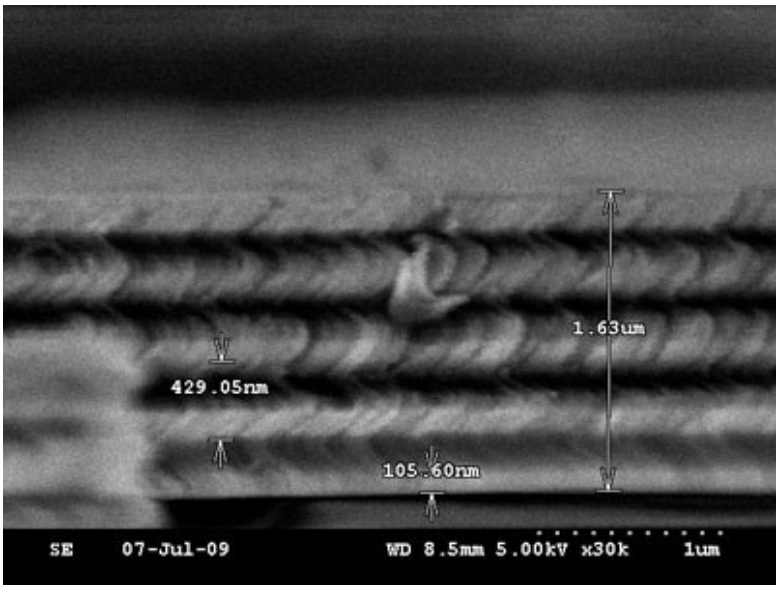

Figure 1.3 SEM image of a chiral STF of magnesium fluoride. (Courtesy: A. Lakhtakia, The Pennsylvania State University).

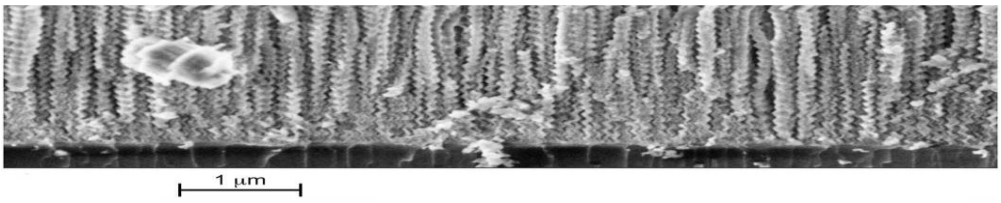

Figure 1.4 SEM image showing the helical nanowires of a chiral STF. (Courtesy: M. W. Horn, The Pennsylvania State University).

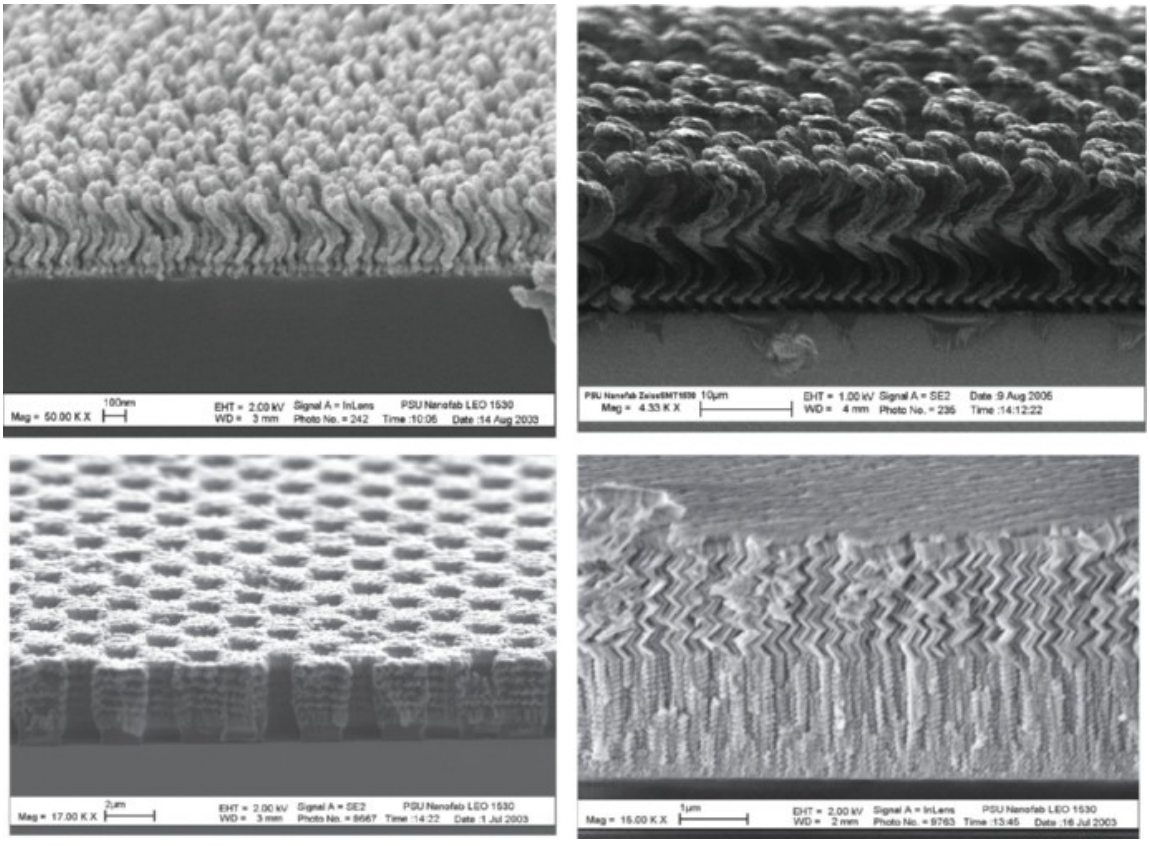

Figure 1.5 Cross-sectional SEM images of STFs. *Clockwise from upper left*: molybdenum STF, parylene STF, two-section STF of silicon oxide, and chiral STF of silicon oxide deposited on a topographically patterned substrate [14].

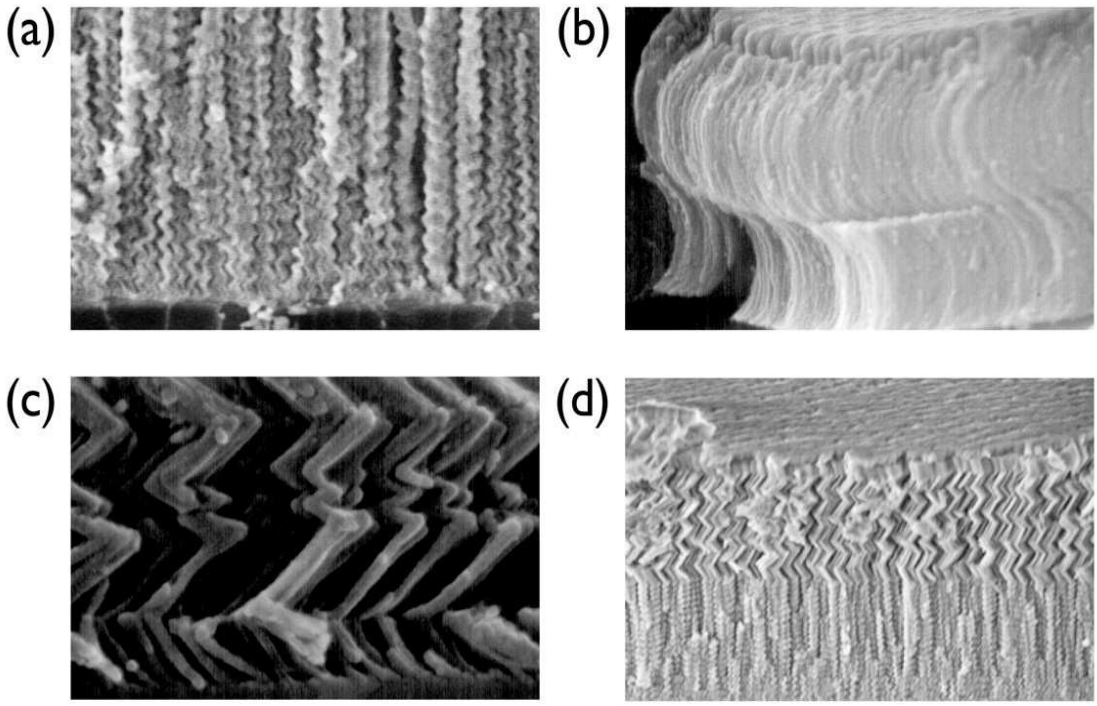

Figure 1.6 Examples of (a) a chiral STF, (b) and (c) sculptured nematic thin films, and (d) hybrid STFs. (Courtesy: M. W. Horn and R. Messier, The Pennsylvania State University).

Many devices using STFs have been fabricated for optical, thermal, chemical, and biological applications. The main area that STF devices have been developed for is optics. The optical properties of STFs have been used widely especially for filter technology, mostly based on exploiting the circular Bragg phenomenon exhibited by chiral STFs [8].

Sculptured thin films have been also suggested for use in integrated circuits as low-permittivity dielectrics [15] and in optoelectronic applications as integrating active light emission and gain elements into sculptured thin films [16].

Probably the first STF was fabricated by Young and Kowal in 1959 [17]. It was a chiral STF, most likely, but its structure had not been determined by electron microscopy Seven years later in 1966, Nieuwenhuizen and Haanstra proved that the growth of columns in a CTF could be altered significantly within a transitional distance of about 30 nm [18]. Then, in 1989 Motohira and Taga showed that by switching the direction of incoming vapor flux, the growth direction could be altered often [19]. Lakhtakia and Messier suggested that arbitrary shaped nanowires can be fashioned by changing the incoming vapor direction during deposition [20]. In 1995, Robbie, Brett and Lakhtakia reported a chiral STF with explicitly designed structure that was verified by SEM images [21]. Since then, STFs have been studied by many researchers. Numerous research papers and book chapters have been written about STFs [22-26].

1.2 The Importance of Surface Plasmon Polariton Waves

An SPP wave is highly sensitive to constitutive disorder near the interface. This feature of SPP waves can be used for many different applications as chemical and biochemical detection systems [1, 30] and imaging systems [31, 32]. Researchers remain focused on various means of exciting and detecting SPP waves [27], binding of recognition molecules to the interface for detecting biomaterials [1], and incorporating surrounding structures to modify the SPP wave [28, 29].

SPP-wave-based chemical and biochemical detection systems have been studied for over two decades. Species such as pesticides, explosives, environmental pollutants, bacteria, viruses, toxins, allergens, and biomedical analytes have been detected [1, 30].

The main disadvantage of any SPP-wave sensor is that it only allows the detection of only one analyte species at a time. Sensing capabilities would increase if more than one SPP waves can be launched at the interface of a metal and a dielectric material.

An emerging approach has been to modify the dielectric partnering material by making it periodically nonhomogeneous normal to the interface. These dielectric materials can be sculptured thin films [3], liquid crystals [33], and rugate filters [34]. The promise of using STFs [3-8] and rugate filters [35] has been investigated theoretically and experimentally.

1.3 What Will Happen If There Are More Than One SPP Waves

Theoretical research has shown that more than one SPP wave can be guided by the same metal/dielectric interface. Multiple SPP waves, of the same frequency but different phase speed, have been experimentally observed at the interface of a metal and a periodically nonhomogeneous STF [5-7].

An STF may have an advantage over dense dielectric materials such as liquid crystals and rugate filters in sensing applications, because it will allow analytes to infiltrate very close to the metal for very sensitive detection and, at the same time, filter out larger undesirable species. Also, an STF can be chemically functionalized to allow only one analyte to bind to it while other species are ignored.

1.4 Outline of Thesis

While the optical response characteristics of CTFs and chiral STFs have been extensively explored theoretically and possible applications have been suggested, very

little experimental research has been conducted on the excitation of multiple SPP waves. For this thesis, in order to comprehensively examine propagation of multiple SPP waves at the planar interface of a metal and a chiral STF, optical experiments were conducted. Different kinds of samples were prepared by first depositing a 30-nm-thick aluminum film on a pre-cleaned glass substrate and then either a chiral STF or a CTF by the thermal evaporation method. The chiral STF could have 3, 4, or 5 periods, each period being 300 nm in thickness. Many methods have been developed to couple an incident light wave to an SPP wave. The Kretschmann configuration, shown in Figures 1.7 and 1.8, which provides the most efficient way to excite SPP waves, was used for the optical experiments. Two kinds of prisms, 45°-90°-45° and hemispherical, were used; all prisms were made of BK7 glass.

The nanoscale morphologies of both CTFs and chiral STFs are discussed in Chapter 2, along with sample preparation and deposition methods. In Chapter 3 measurement techniques, the Kretschmann configuration and a commercial prism-coupler set-up, are described. Two different types of prisms (45°-90°-45° and hemispherical) used in the Kretschmann configuration are introduced. The relevant chemical and optical properties of materials (aluminum, sodium fluoride, magnesium fluoride, and zinc selenide), which were used to deposit metal thin films, CTFs, and chiral STFs, are provided in Chapter 4. The graphs of reflectance vs. angle of incidence are shown in Chapter 5, and discussed in detail. Chapter 6 draws together the conclusions of the previous chapters and contains suggestions for future work.

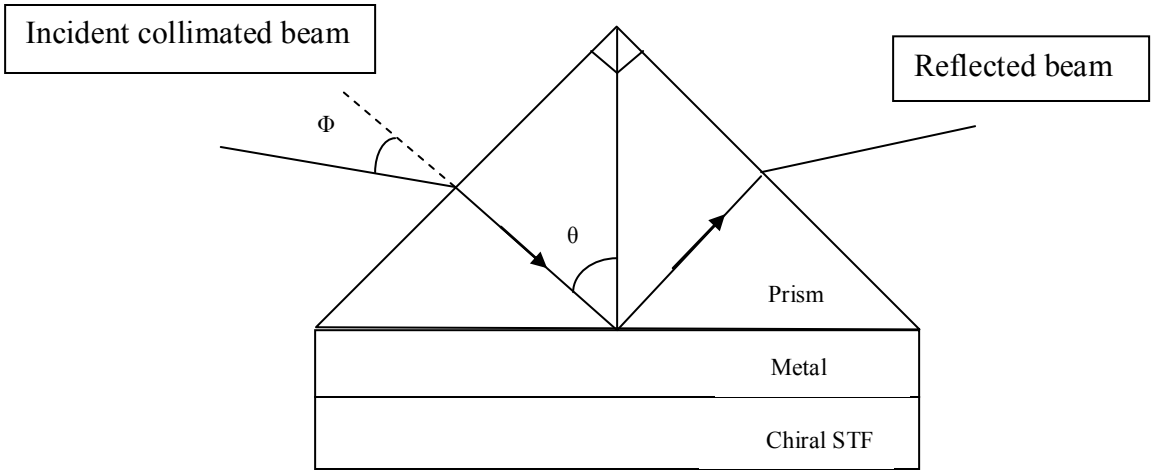

Figure 1.7 Schematic of the Kretschmann configuration (45°-90°-45° prism). The prism must be made of an isotropic dielectric material of refractive index greater than the maximum principal refractive index of the chiral STF.

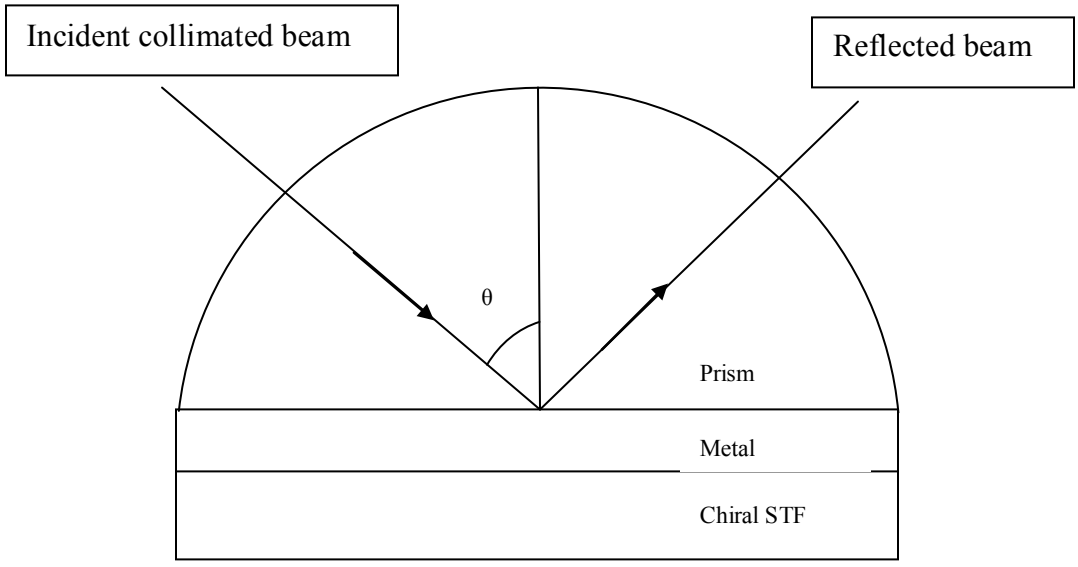

Figure 1.8 Schematic of the Kretschmann configuration (hemispherical prism).

CHAPTER 2

Sample Fabrication

The morphologies and growth mechanisms of columnar thin films (CTFs) and chiral STFs are discussed in this chapter along with a brief history of thin-film morphology and thin-film fabrication techniques. The steps followed to deposit desired thin films for experiments for the excitation of multiple SPP waves are also presented. Thermal evaporation was used for all thin films.

2.1 History of Thin-Film Morphology

Many studies on thin-film coatings fabricated using physical vapor deposition (PVD) investigated their optical properties. In 1857, Faraday realized the similarity between the optical properties of gold colloids and thermally evaporated coatings of gold [36]. Then in 1886, Kundt proposed a relation between the anisotropic optical properties of CTFs of a metal deposited using an obliquely directed flux of an evaporant in vacuum with respect to substrate plane [37].

By 1950 König and Helwig [38] had used a directional vapor flux, specifically for evaporation at low pressure and the low adatom-mobility, which results in self-shadowing at the 10-to-100-nm length scale. They demonstrated the development of ~100-nm particles by the capture of obliquely incident vapor particles (adatoms) and creating regions with no deposited particles. Soon thereafter, Holland used the self-shadowing concept to explain the light-scattering characteristics of obliquely deposited metal films

[39]. In his book, published in 1956 [40], the studies of König and Helwig were summarized and the conceptual model of the growing CTFs consisting of cylindrical columns with dome-shaped tops were presented.

During the 1960s, Movchan and Demchishin introduced the concept of "structure zones" [41] in order to classify the top surfaces and the cross-section morphologies of thermally evaporated metal and oxide films. They created a structure zone model (SZM) which developed over the next several decades. An SZM is shown in Figure 2.1. In Zone 1, which is of interest for STFs because of low adatom-mobility conditions, tapered grains define the morphology. In Zone 2, straight-sided columnar crystalline grains are formed due to higher temperatures, which permit surface diffusion of adatoms. In Zone 3, grain size increases and columnar morphology is no longer present.

The relations between deposition conditions, morphology, and optical properties were not well understood prior to the development of characterization tools and optical theories that take nanoscale morphology into account between the 1940s and 1970s. The development of transmission electron microscopes (TEMs) allowed the viewing of film structure at the nanoscale and helped explain the anisotropic optical properties of CTFs [43]. In the 1970s, scanning electron microscopes (SEMs) became widely used tools to characterize thin-film morphology.

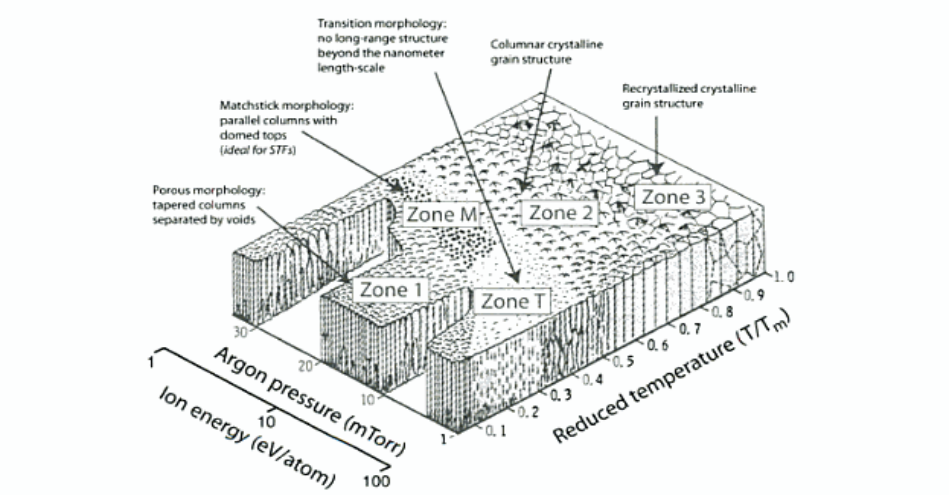

Figure 2.1 A current version of the SZM [42]. The variables are reduced temperature (T/T_m), where T is the substrate temperature and T_m is the melting point of bulk material, the argon gas pressure in the chamber, and the ion bombardment energy.

With extensive study of electron microscope images, Thornton extended the original SZM and included a transition zone (Zone T) between Zones 1 and 2 [44]. In Zone T, the growth is characterized by grains with fine-domed tops. Experimental studies [45-50] and computer simulations [51, 52] conducted between the 1960s and 1970s, demonstrated the existence of void networks and columns of 10-to-20-nm-diameter for low adatom-mobility conditions. By the early 1980s, Messier and colleagues [53-60] explained the evolution of morphology as a function of film thickness, thereby connecting the atomic-level understanding of self-shadowing and the SZM. They presented a cluster-based model to explain the change from Zone 1 to Zone T [53, 61, 62]. A new zone called Zone M was identified. Knowledge of this zone is extremely important to fabricate STFs.

The anisotropy of self-shadowing for oblique deposition was also confirmed by other studies [63-65]. By the early 1990s, Motohiro and Taga [66] showed the instantaneous change of the direction of columnar growth is possible. Since the fundamental building blocks of thin film morphology are 1-to-3-nm clusters, instantaneous change of direction at those length scales is possible, which enables the deposition of STFs [42].

2.2 Morphology and Growth Mechanism of Columnar Thin Films

The growth of oblique-angle CTFs by PVD is generally credited to Kundt [67]. The source material is evaporated from a tungsten boat in a chamber, while the substrate is at low temperature and the chamber is under vacuum. The substrate is held at a fixed angle with respect to the incoming vapor flux. The angle between the direction of the incoming vapor flux and the substrate plane is denoted by χ_v. The arriving atoms form 1-to-3-nm clusters on the substrate. When the substrate temperature is below a third of the source material's melting temperature, the nucleation clusters evolve into cone-shaped columns [53].

Columnar thin films are thus the direct result of self-shadowing, and are grown under low adatom-mobility conditions by either evaporation from a point source or sputtering from a planar source. The CTF morphology can be controlled during growth by changing the direction of incoming vapor flux [10]. The columnar structure also can be affected by rapidly rotating the substrate during deposition [42]. CTFs can be grown from basically any type of material that can be evaporated.

2.3 Morphology and Growth Mechanisms of Chiral STFs

The growth of chiral STFs is credited to Young and Kowal [17]. They were the first to engineer growth of STFs with three-dimensional morphology. They deposited calcium-fluoride thin films, with morphology predicted to display transmission optical activity, by rotating the substrate about the central normal axis (z axis) constantly during growth. Even though Young and Kowal realized the columnar direction could be altered by continuous or instantaneous rotation of the substrate, the morphology of the deposited films was not confirmed via scanning electron microscopy. Robbie *et al.* confirmed the helicoidal morphology of the films that were deposited by rotating the substrate [21, 68].

Thus, chiral STFs are produced by rotating the substrate about its surface normal to produce helical nanocolumns, which result from a constant rotation rate [10, 21].

2.4 Deposition Methods

Several methods are used to deposit thin films: physical deposition, chemical deposition, and other methods using both physical and chemical deposition methods. In chemical deposition, a chemical reaction occurs in order to form a solid surface. It can be categorized by the phase of precursor as chemical solution deposition (CSD), chemical vapor deposition (CVD) and plasma-enhanced CVD. Physical deposition uses mechanical or electrochemical changes to form a thin film. Thermal evaporation, sputtering, and pulsed laser deposition (PLD) are some examples of physical deposition. Molecular beam epitaxy (MBE) deposition is a combined physical and chemical process.

The deposition of STFs requires low substrate temperature and a directional vapor

flux, so that the desired top surfaces, which depend on self-shadowing effects of arriving adatoms, can be formed. The methods to deposit STFs are the following PVD methods:

(i) Thermal evaporation [40, 69, 70],

(ii) Sputtering [10, 71], and

(iii) Pulsed laser deposition [72].

The majority of reported STFs were deposited by thermal evaporation method; however, a few were prepared by sputtering and pulsed laser deposition. The possible high deposition rate makes the thermal evaporation method very desirable to fabricate practical STFs.

Thermal evaporation is a physical process that requires the evaporation of a source material in vacuum. Even though it is mostly used for depositing metal films, thermal evaporation is also a suitable method to deposit CTFs and chiral STFs made of inorganic materials, although it has some disadvantages such as out-gassing of hot source material, contamination, and alloy formation.

There are advantageous features of thermal evaporation, too. For example, the evaporated atoms have a Maxwellian energy distribution, determined by the temperature of the source, which reduces the number of high-speed adatoms that can cause deformation of the thin film being deposited. The method provides a constant deposition rate and high purity. Also, any material that can be evaporated is suitable to be used as a source material, which broadens the usage of the method. Due to these advantages,

thermal evaporation method was chosen to deposit metal thin films as well as columnar and chiral STF samples. The thermal evaporation system used in this study is shown in Figure 2.2.

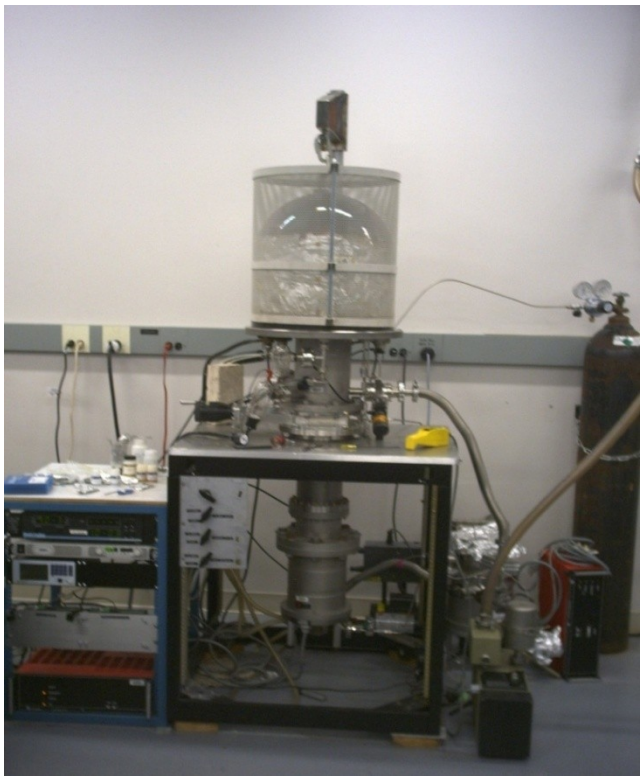

Figure 2.2 Thermal evaporation system used for making all thin films reported in this thesis.

A typical thermal evaporation system has a high-vacuum chamber, a boat containing the source material, and a substrate. When the boat is heated, the vapor pressure of the evaporant becomes substantial. Hence, evaporated adatoms are released into the vacuum chamber and some of these adatoms reach the substrate to form a film.

Usually, resistive heating is used to evaporate a source material onto a given substrate. Films with a specified thickness of up to several microns can be deposited. The thickness is measured *in situ* by a quartz crystal monitor (QCM). Typical crystal heads are shown in Figure 2.3 and a QCM is shown in Figure 2.4.

Figure 2.3 Typical crystal heads used in QCMs (Kurt J. Lesker Company, http://www.lesker.com).

Figure 2.4 Ouartz crystal monitor [http://www.tectra.de].

The first step to prepare a sample for optical experiments was to deposit an aluminum film approximately 30 nm in thickness on a pre-cleaned glass slide. The aluminum film was deposited by thermal evaporation and the thickness was monitored *in situ* by a QCM. Prior to deposition, the vacuum chamber was pumped down to a base pressure of ~10^{-6} Torr. In order to evaporate the source material, a current of ~32 A was passed through a tungsten boat (shown in Figure 2.5) containing bulk aluminum. The glass slide was located normal to the incoming aluminum vapor flux ($\chi_v = 90°$). During deposition, the substrate holder was rotated about the axis passing normally through its surface at a constant angular speed of 2 rps.

Figure 2.5 Evaporation boats (Kurt J. Lesker Company, http://www.lesker.com).

Following the deposition of aluminum, either a magnesium fluoride CTF or a chiral STF (of sodium fluoride, zinc selenide or magnesium fluoride) was deposited.

To obtain columnar morphology, the substrate was held at an oblique angle which is measured between the direction of incoming vapor flux and the substrate plane. The oblique angle, referred as χ_v, is shown in Figure 2.6. For this study, χ_v was fixed at either 10° or 15°. To obtain a chiral morphology, the substrate was stepwise rotated about the normal axis at 18°/step with a 54.25 s break between steps. The chiral STFs fabricated were of 3, 4, or 5 periods, each period being 300 nm in thickness.

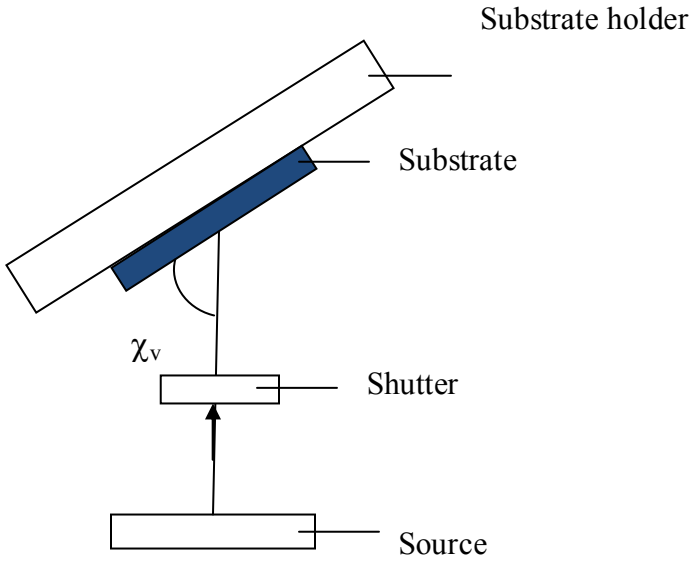

Figure 2.6 Schematic to show the incoming vapor flux angle (χ_v).

The substrate orientation was controlled by a computer program. The substrate holder was fixed at a desired χ_v and rotated by a stepper motor. A constant deposition rate was maintained and controlled by monitoring thin film thickness using the QCM. The current passing through tungsten boat was adjusted for a constant deposition rate.

Once the required thickness was reached, a shutter was closed to prevent the vapor flux from reaching the substrate. Before taking the sample out of the vacuum chamber, a cool-down time was needed which was estimated as about half of the deposition time.

SEM images of samples were taken to ensure the columnar/chiral morphology and the quality of deposited thin films. An SEM image showing a zinc-selenide chiral STF is provided in Figure 2.7.

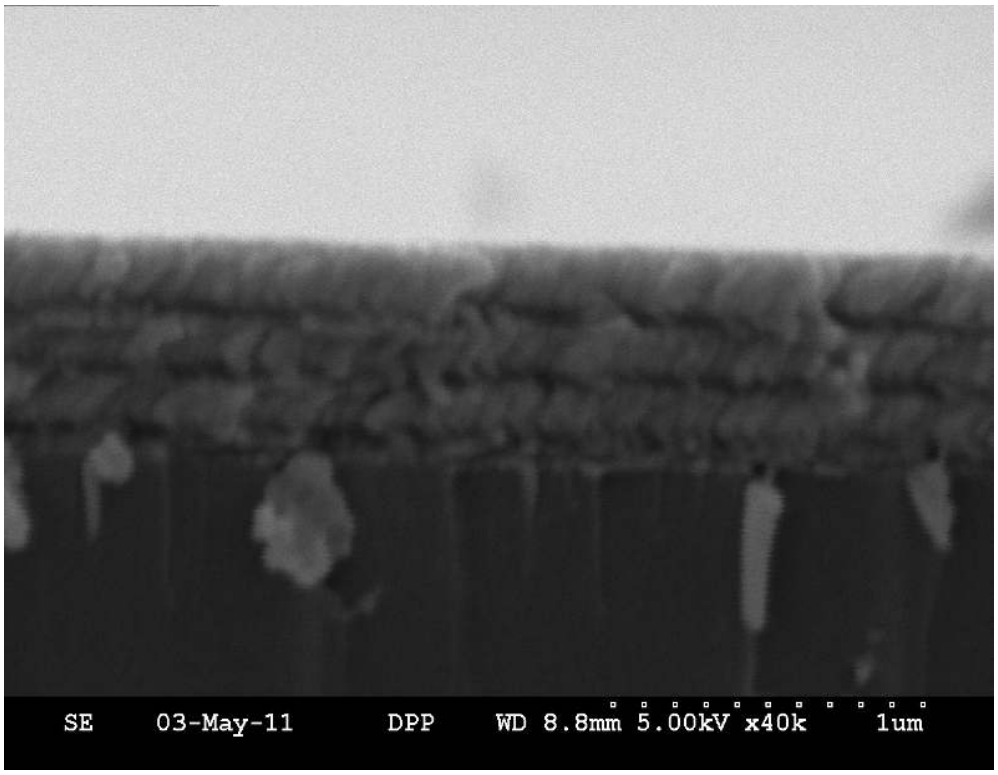

Figure 2.7 SEM image of a chiral STF made by evaporating zinc selenide (Courtesy: Drew P. Pulsifer.)

2.4.1 Tooling Factor, Density and Z-ratio

A quartz crystal was used to measure the thickness of the deposited thin film. The quartz crystal oscillates at a resonant frequency which depends on the thickness of the deposited film. A QCM can measure the thickness of a single atomic layer with 0.5% accuracy [38]. The life of a quartz crystal is dependent on the deposition conditions such as its location and the rate of evaporation, as well as on the evaporant materials. The quartz crystal must be replaced frequently to have consistent results.

The position of the QCM in the evaporation chamber affects the monitoring data. In order to calibrate the QCM with respect, a position tooling factor is used.

The density and the Z-ratio of the source material are important factors to measure the thickness precisely. The Z-ratio is used to correct the frequency change to a thickness transfer function. The correction is needed for the effects of acoustic-impedance mismatch between the source material and the crystal [39].

The density of the deposited material changes with χ_v. To avoid any possible error, densities for normal incidence ($\chi_v = 90°$) were used for all values of χ_v, with the tooling factor adjusted to compensate for change in density.

The tooling factors, density and Z-ratio of the deposited materials for this study are provided in Table 2.1.

Materials	Tooling Factor (%)		Density (g/cm^3)	Z-Ratio
Aluminum	400		2.7	1.08
Magnesium fluoride (MgF_2)	200		3.18	0.637
	$\chi_v = 10°$	$\chi_v = 15°$		
Sodium fluoride (NaF)	135	200	2.56	0.949
Zinc selenide (ZnSe)	135	200	5.49	0.722

Table 2.1 Tooling factor, density and Z-ratio of materials used to fabricate thin films.

2.5 Sample Fabrication

Thin films were deposited on pre-cleaned glass slides. First, the glass slides were cut in to approximately 2 cm × 2 cm pieces for samples for the Kretschmann configuration and 0.5 cm × 1 cm for the commercial prism-coupler set-up. The glass slides were then sonicated for 10 min each side. If further cleaning was necessary, they were cleaned by hand using ethanol and deionized water. After the cleaning process, glass slides were attached to a substrate holder which is a plate placed in the vacuum chamber. The glass slides were positioned as close as possible to the center of the substrate holder for a reasonable uniformity in the film thickness.

CHAPTER 3

Optical Measurement Techniques

In this chapter, optical measurement techniques and the steps followed to collect optical data are presented. Three different experimental set-ups were used to detect the excitation of surface-plasmon-polariton waves in this study.

All three set-ups were based on the Kretschmann configuration [73]. The first two set-ups (Set-up #1 and Set-up #2) were implemented on an optical bench, while Set-up #3 was a commercial device. The Kretschmann configuration uses a high-refractive-index prism to couple incident light to a metal/dielectric interface, in order to excite SPP waves if possible. In Set-up #1 and Set-up #3, 45°-90°-45° BK7 prisms were used, but a hemispherical BK7 prism was used in Set-up #2.

3.1 Set-up #1

An optical system, shown schematically in Figure 3.1, was used to measure the reflectance from the prism/glass-slide/metal/STF structure. The uncoated side of the glass slide was affixed to the hypotenuse of a 45°-90°-45° BK7 prism by using Cargille-type NVH immersion oil for refractive-index match. The refractive index of the prism glass is 1.515090 [74]. The prism was mounted on a Newport 481 rotary stage.

A 633-nm He-Ne laser (LHRP-1201, Research Electro Optics) was used as the light source to illuminate the sample. The laser was turned on approximately 30 min before use, in order to stabilize the incident light. Measurements were made for both p- and s- states of polarization of the laser beam. An indicator arrow on the laser and a polarizer were used to choose the polarization state. If the arrow on the laser points upwards it indicates that the light is s polarized. For p polarization, the arrow is positioned to the right side of the laser. A polarizer was placed between the laser and a rotary stage on which the prism/glass-slide/metal/STF structure was placed. For p polarization the angle on the polarizer was set to 1°, and for s polarization 91°. The intensity of the incident light was measured as a voltage by a photomultiplier detector to later calculate the intensity ratio of reflected light to the incident light. Then the photomultiplier detector was used to measure the light reflected by the prism/glass-slide/metal/STF structure. In order to alter the angle of incidence (Φ in Figure 3.1) of the light falling on the structure, the entire assembly was rotated in 0.25° steps between -25° and 40°. The angle Φ read on the rotary stage was converted to the angle of incidence (θ) on the metal/STF interface. The overall reflectance and the transmittance up to total internal reflection were detected by a PDA 36A (Thor Labs.) photomultiplier detector. Tektronix TDS 2024B oscilloscope was used to read the voltage from the photomultiplier detector. The experimental set-up is shown in Figures 3.2 and 3.3.

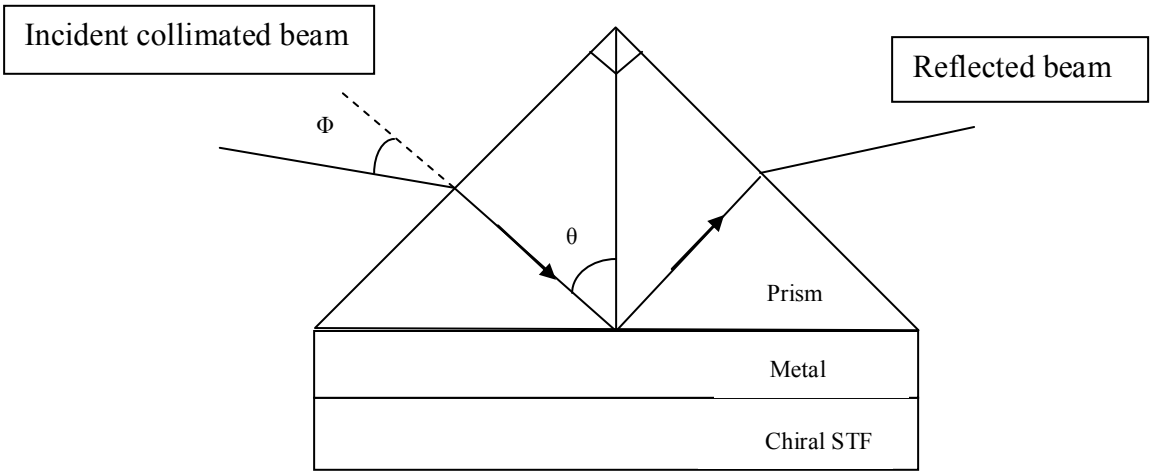

Figure 3.1 Kretschmann configuration with 45°-90°-45° prism (Set-up #1).

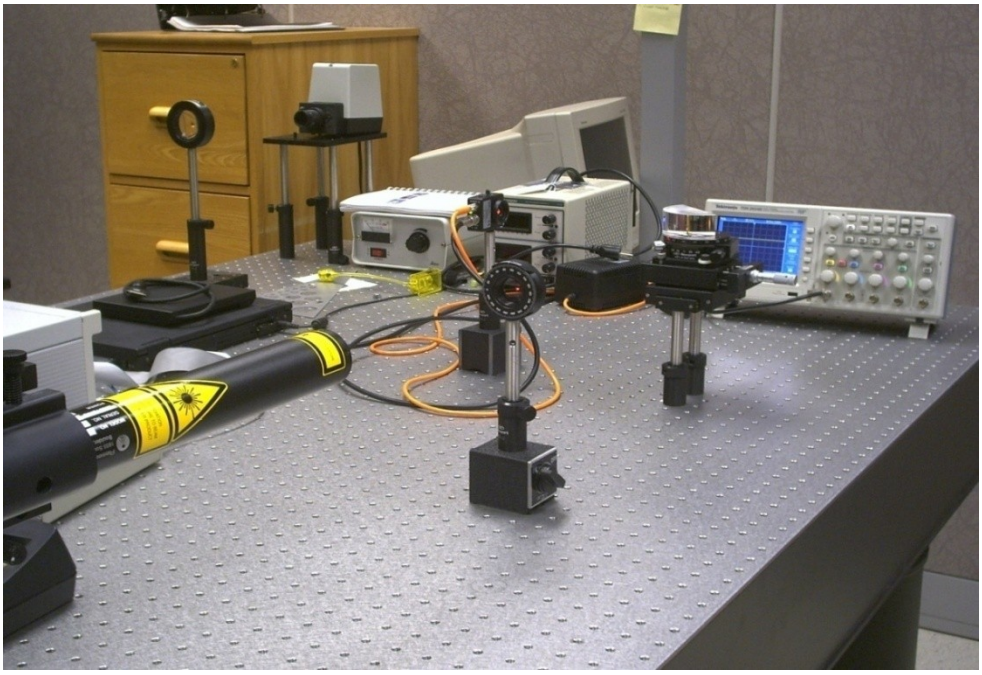

Figure 3.2 Kretschmann configuration set-ups on an optical table.

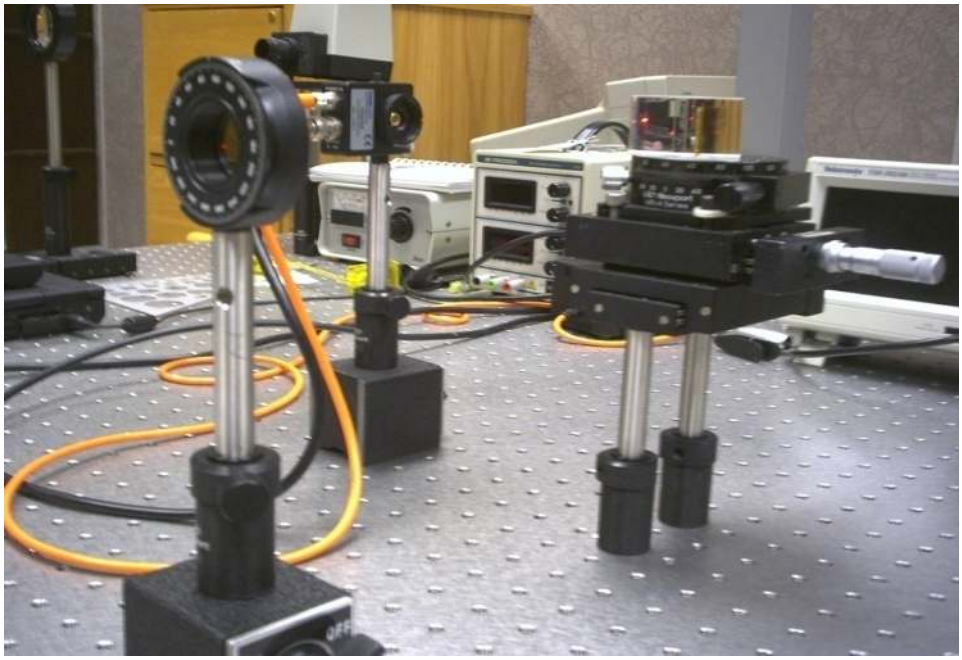

Figure 3.3 Close-up of Figure 3.2 to show rotary stage, photomultiplier detector and polarizer.

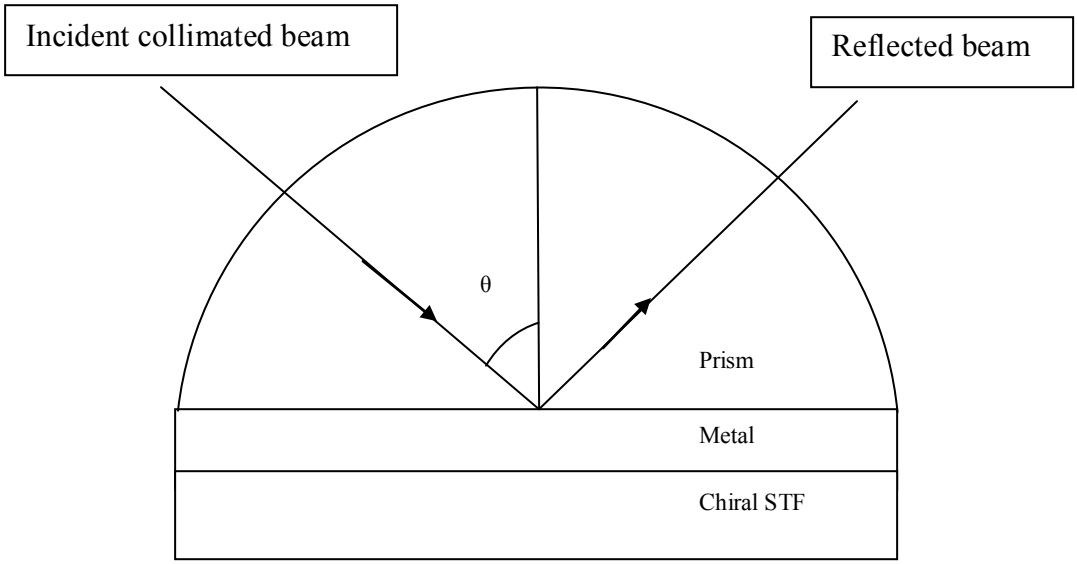

Figure 3.4 Kretschmann configuration with hemispherical prism (Set-up #2).

3.2 Set-up #2

Set-up #2 is identical to Set-up #1, except that a hemispherical prism was used to allow a wider range of the angle θ; see Figure 3.4. By using a prism of this shape converting an external angle Φ to θ was not necessary. The angle which was read on the rotary stage was the same as the angle of incidence on metal/STF interface. The dimensions of the prism were designed to match with the rotary stage. The dimensions of the hemispherical prism are shown in Figure 3.5. The hemispherical prism was custom-manufactured by Jenoptik [http://www.jenoptik.com].

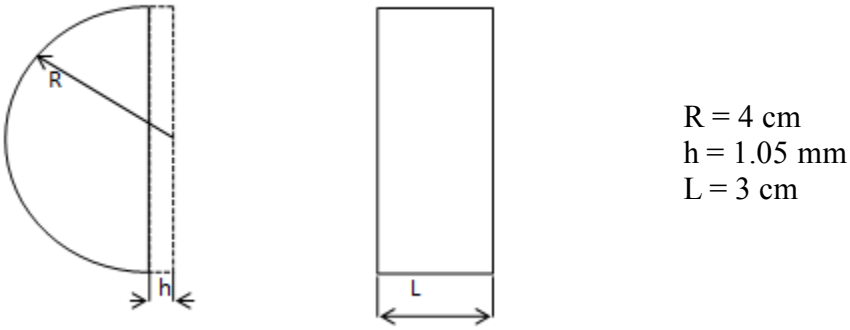

Figure 3.5 Hemispherical prism used in Set-up #2.

3.3 Commercial prism-coupler set-up (Set-up #3)

A commercial prism-coupler instrument manufactured by Metricon Company was used as Set-up #3 (model no. 2010/M). There are three component modules in this instrument:

1. Optics: laser, rotary stage, prism, photomultiplier detector, and other components.
2. PC: displays, analyzes mode patterns, and calculates results.
3. Interface module: connect the optics module and PC, stepper motor drive electronics.

The sample was brought into intimate contact with the prism by using immersion oil. Then the prism was placed on the rotary stage. The most important part of positioning the prism is to avoid touching the photodetector. A 633-nm laser was used as the light source which was turned on sufficiently in advance. The laser spot was aligned onto the prism. The computer was turned on and the Metricon program was started. After the program was opened, values such as substrate's refractive index, prism code, and scan limits were entered in parametric form. In general, default values for detection limits were used. The rotary stage on which the prism is mounted was referenced automatically by simply clicking AutoRef which aligns the rotary stage with incident light automatically. A pattern of two sharp peaks would appear on the screen. Thereafter, the rotary stage was

turned manually by using +/- speed control on the interface box to adjust the gain. The gain was set to the maximum value when the highest peak was hit. The whole θ-range was scanned by clicking Auto Scan which scans the selected range of angles automatically. The commercial prism-coupler set-up is shown in Figure 3.6.

3.3.1 Metricon Prism Coupler Steps:

1. Sample loading: A sample is brought into intimate contact with the prism by immersion oil which is used for refractive-index match. The prism is placed in the clamp by using screws. Then the clamp is put on the rotary stage. One should be careful while placing the prism and avoid hitting the detector.

2. Turn on the laser and orient the wavelength label horizontal. The laser spot must be aligned onto the prism.

3. Turn the computer on, log in, and start the program Metricon.

4. When the program starts, enter the values of substrate's refractive index, prism code (written on the prism case), and scan limits (generally use default settings).

5. Either p or s polarization of light has to be chosen for data collection.

6. Reference the rotary stage automatically by clicking AutoRef. A pattern of two sharp peaks should appear on the screen.

7. Move the rotary stage manually by turning the +/- speed control on the interface box. Adjust gain at peak of maximum to almost the maximum value.

8. Click AutoScan.

9. Once the graph is plotted, the data can be saved into a folder, which is then copied in an external memory.

10. After the data is saved, the computer is shut down.

11. The laser and the interface box are turned off.

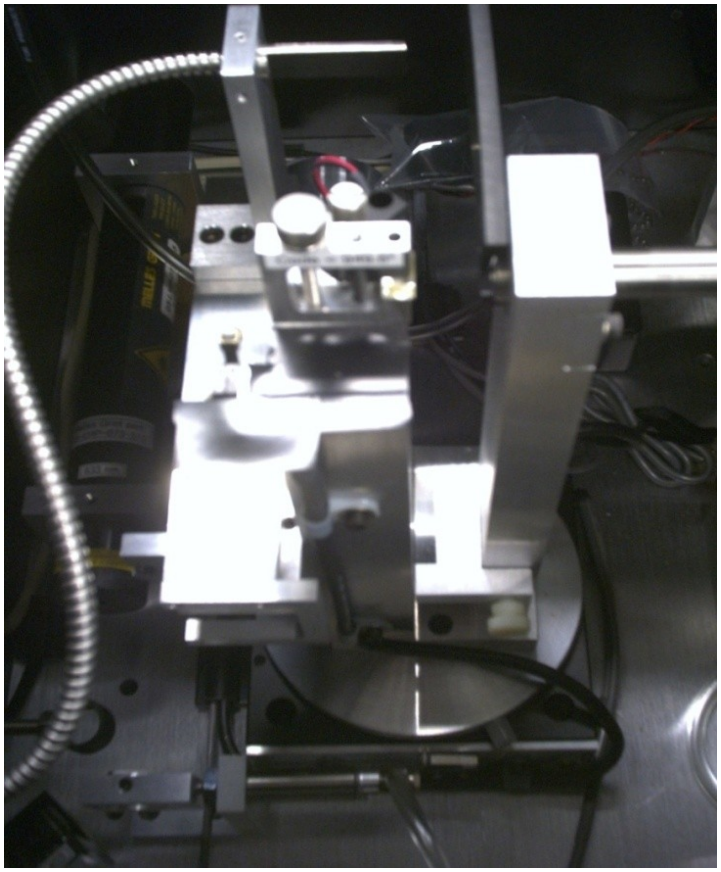

Figure 3.6 Commercial prism-coupler set-up (Set-up #3) (Metricon Company, model no. 2010/M).

CHAPTER 4

Materials

In this chapter, materials used to deposit thin films and optical properties of these materials are presented: aluminum (Al), sodium fluoride (NaF), magnesium fluoride (MgF_2), and zinc selenide (ZnSe) used. These materials were chosen according to their bulk refractive indexes, shown in Table 4.1.

Aluminum was deposited as ~30-nm-thick films on glass substrates. Then on the top of aluminum film either a CTF or a chiral STF of an inorganic material was deposited. The thickness of the inorganic thin film ranged between 900 nm to 1500 nm.

Material	Refractive Index
BK7 glass	1.51512
Aluminum	1.37+10.2 i
Magnesium fluoride	1.377
Sodium fluoride	1.32455
Zinc selenide	2.59123

Table 4.1 Bulk refractive indexes of materials at 633-nm wavelength [74].

Material	Base Pressure (Torr)	Melting Temperature (°C)
Aluminum	1.9×10^{-5}	660
Magnesium fluoride	5.6×10^{-6}	1262.7
Sodium fluoride	1.2×10^{-5}	992.7
Zinc selenide	5.1×10^{-6}	1525

Table 4.2 Base pressure and melting temperature for evaporation of different materials used in this research.

4.1 Aluminum

Preparation:

The glass slide was cleaned in an ultrasonic bath for 10 min for each side, and then with hand by using ethanol and deionized water. The glass slide was placed on the

substrate holder which is used in the vacuum chamber.

Deposition:

Aluminum was deposited on the glass substrate by the thermal evaporation technique. The approximate thickness of the thin film was 30 nm, as measured by the QCM.

Optical Data:

Optical data were recorded for the prism/glass-slide/aluminum structure. The laser was turned on for at least 15 min before use. The data were collected for both p and s polarizations of the incident light. The arrow on the laser indicates the polarization. For p polarization, the arrow points rightward and the angle on the polarizer is 1°. For s polarization, the arrow points upwards and the angle of the polarizer is 91°.

The sample was mounted on the prism by using immersion oil which was used for matching the refractive indexes of the prism and the glass slide. The voltage of the incident light was measured by a photo detector and the value was recorded.

Measuring the reflectance for different values of θ was the basis of the experiments. The data were collected approximately for $-8° \leq \Phi \leq 9°$ which was read from the rotary stage. From Φ, θ was calculated according to the formula;

$$\theta = 45° + \sin^{-1}\left[\frac{\sin\Phi}{1.515090}\right].$$

Thus, $\Phi = -8°$ yields $\theta = 39°$, and $\Phi = 9°$ yields $\theta = 50°$.

Analysis:

The line graphs showing reflectance depending on θ were used to analyze the data. The graphs were plotted for both p and s polarizations. A reflectance minimum for p polarization and a quasilinear curve line for s polarization was the expected behavior of the graphs [75, 76].

Notes:

The experiment should be done right after the sample is deposited. Metal films are subject to oxidation. The quality of the film may reduce with time very rapidly.

4.2 Magnesium fluoride (MgF_2)

Magnesium fluoride is an inorganic chemical compound. It is transparent for a wide range of wavelengths and is commercially used in optics. CTFs of magnesium fluoride were deposited on aluminum thin films with different thicknesses. The data were taken for both p and s polarizations of the incident light on Set-up #1.

4.3 Sodium fluoride (NaF)

Sodium fluoride is an inorganic chemical compound. Chiral STFs of sodium fluoride were deposited on aluminum thin films. These chiral STFs were of 3, 4, or 5 periods, each period being 300 nm in thickness. The measurements were done for both p and s polarizations of the incident light on Set-up #1.

4.4 Zinc selenide (ZnSe)

Zinc selenide is a light, yellow solid compound which is rarely found in nature. It is an intrinsic semiconductor. Three, four and five periods of chiral STFs of ZnSe were deposited on aluminum thin films. The measurements of reflectance were made using Set-up #2 and Set-up #3.

CHAPTER 5

Experimental Results for Multiple SPP Waves

In this chapter experimental results for the excitation of multiple SPP waves are presented. The measured photodetector voltage for incident light is denoted by U_{inc} and the measured photodetector voltage for the reflected light is indicated by R. The graphs showing the reflectance R/U_{inc} of the incident light versus the angle θ were plotted. Along with these graphs, the reflectance minimum points, which can be evidence for excited SPP waves, are presented in tables. The results were classified according to thickness of the deposited STFs, the linear polarization state of incident light (p-polarized or s-polarized), and the set-ups used to collect data. The arrows in the graphs indicate the reflectance minimum points.

5.1 Glass-slide/Aluminum Structure

A 30-nm-thick aluminum film was deposited on a glass substrate. The optical data were taken for both p and s polarizations of the incident light by using Set-up #1. (For data see Table A.1 in the Appendix).

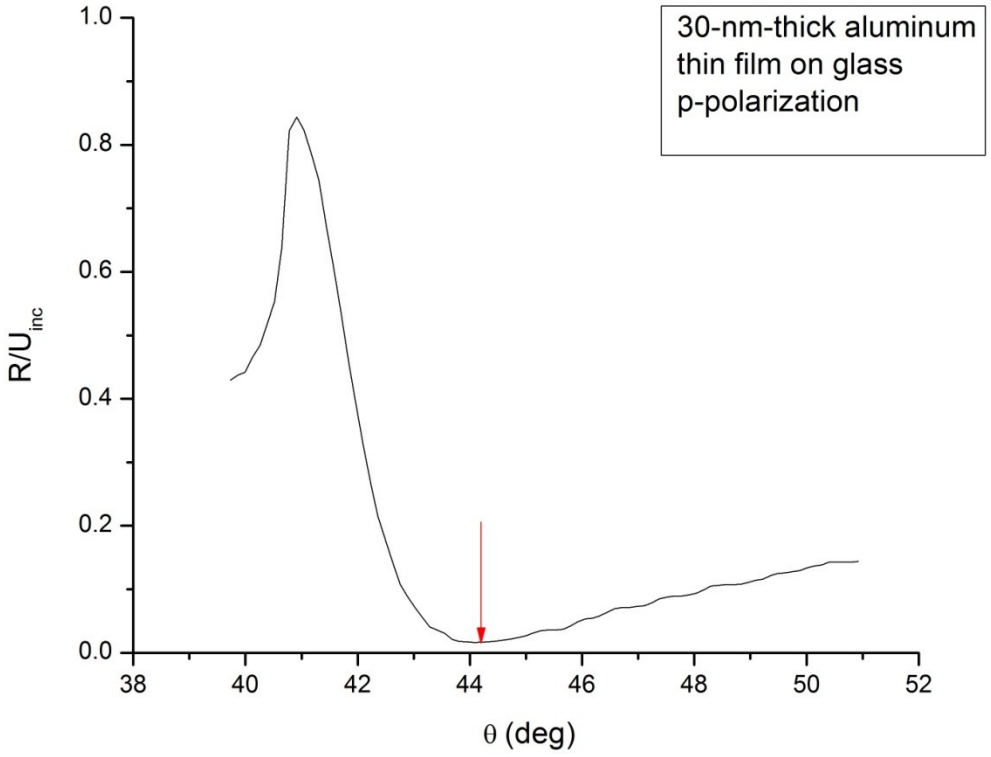

Figure 5.1 Measured reflectance R/U_{inc} as a function of the angle of incidence θ, for a 30-nm-thick aluminum thin film. The incident plane wave is p-polarized and the free-space wavelength is 633 nm. The Kretschmann configuration with a 45°-90°-45° prism (Set-up #1) was used.

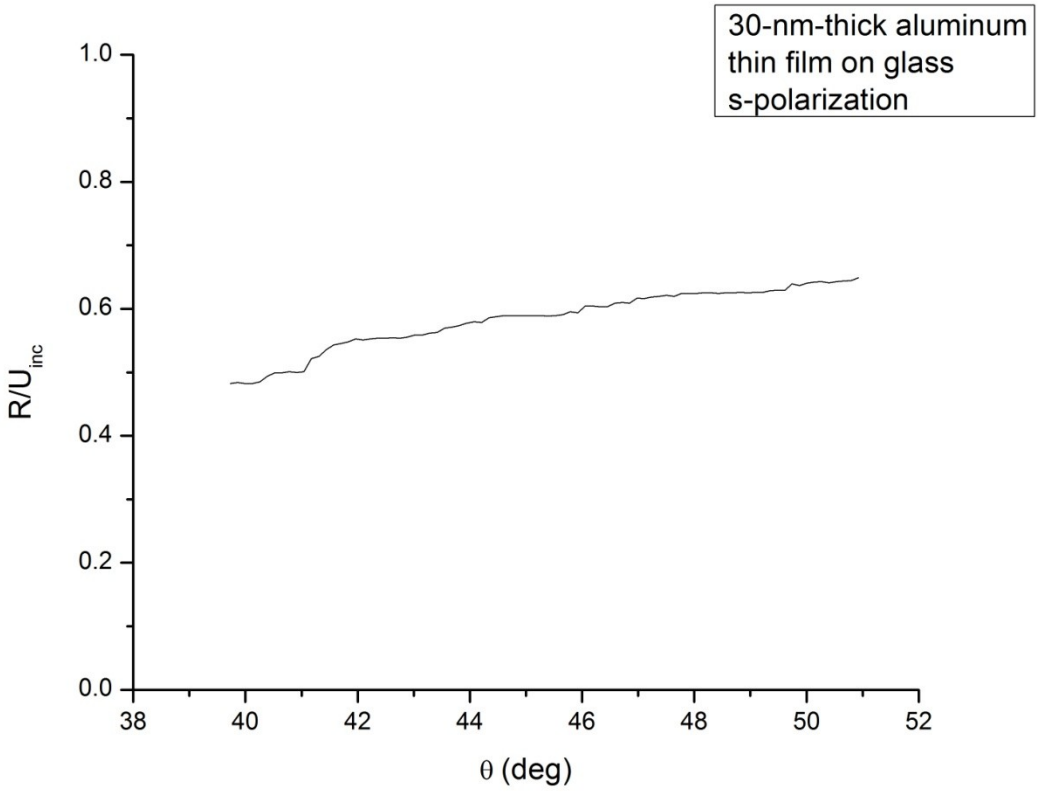

Figure 5.2 Same as Figure 5.1 except that the incident plane wave is s-polarized.

The data presented in Figure 5.1 show that there is a reflectance minimum for p-polarized incident light at $\theta = 44.20°$. In contrast, for s-polarized incident light there is no reflectance dip in Figure 5.2; instead, the reflectance increases as θ increases. These results are well matched with the previous experiments of others [75] as well as with theory [3, 76].

5.2 Glass-slide/Aluminum/MgF_2-CTF Structure

Columnar thin films of magnesium fluoride were deposited on 30-nm-thick aluminum in a thermal evaporation system. Two different samples, with 1200-nm- and 1600-nm-thick CTFs deposited at $\chi_v = 15°$, were fabricated. Optical data were taken by using the Kretschmann configuration with 45°-90°-45° prism (Set-up #1), and are presented in Figures 5.3-5.6 and Table 5.1. (For data see Table A.2 in the Appendix).

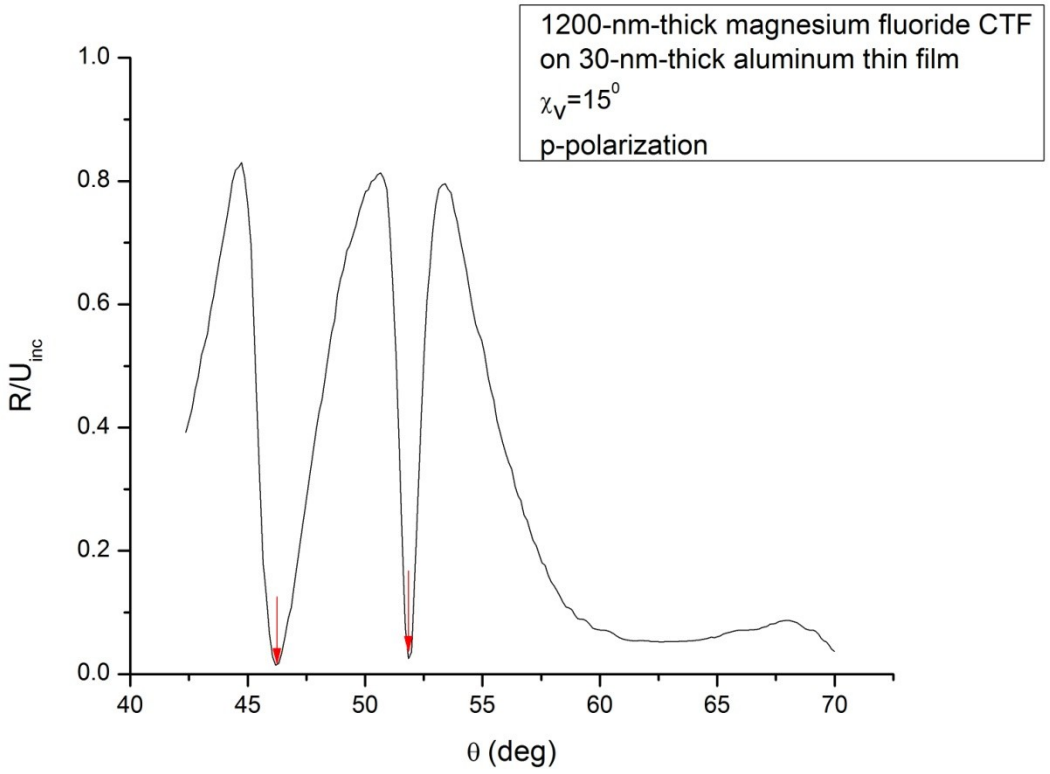

Figure 5.3 Measured reflectance R/U_{inc} as a function of the angle of incidence θ, for a 1200-nm-thick magnesium fluoride CTF on a 30-nm thick aluminum film. The incident plane wave is p-polarized and the free-space wavelength is 633 nm. The Kretschmann configuration with a 45°-90°-45° prism was used (Set-up #1).

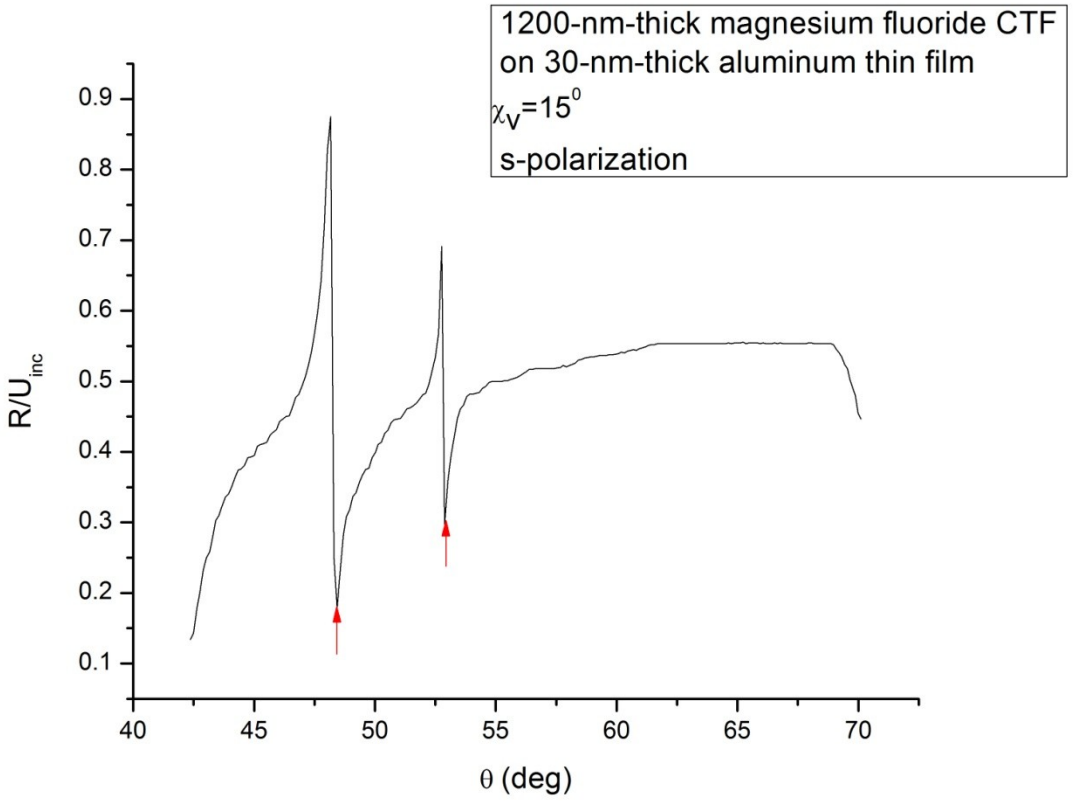

Figure 5.4 Same as Figure 5.3 except that the incident plane wave is s-polarized.

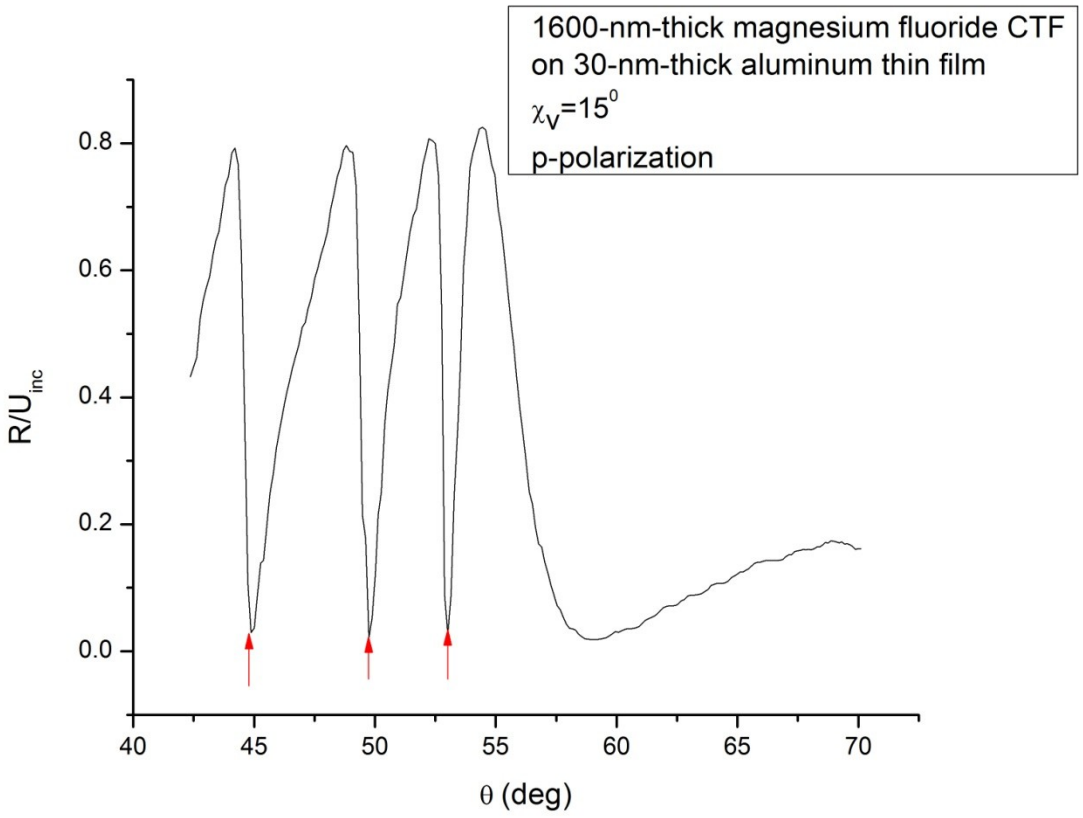

Figure 5.5 Measured reflectance R/U_{inc} as a function of the angle of incidence θ, for a 1600-nm-thick magnesium fluoride CTF on a 30-nm-thick aluminum film. The incident plane wave is p-polarized and the free-space wavelength is 633 nm. The Kretschmann configuration with a 45°-90°-45° prism was used (Set-up #1).

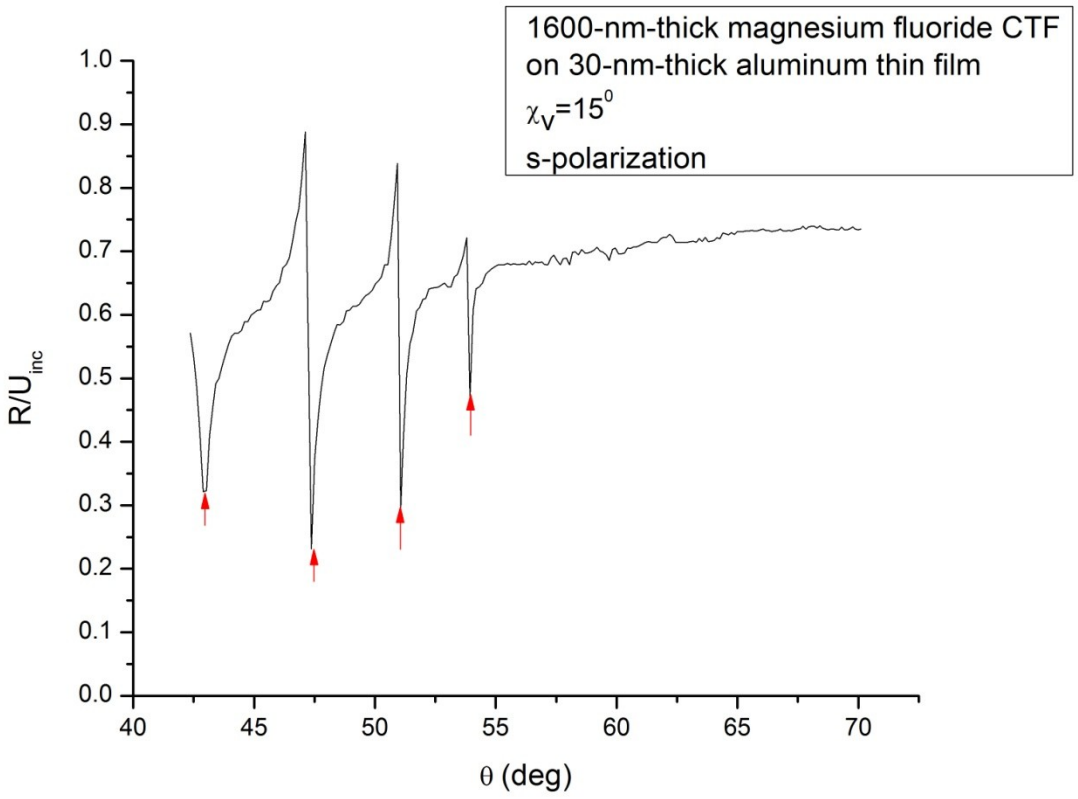

Figure 5.6 Same as Figure 5.5 except that the incident plane wave is s-polarized.

Thickness of the CTF	1200-nm		1600-nm			
Polarization of incident light	First dip	Second dip	First dip	Second dip	Third dip	Fourth dip
p	46.31°	51.84°	44.86°	49.74°	53.01°	
s	48.42°	52.88°	43.02°	47.37°	51.05°	53.92°

Table 5.1 Reflectance minimums for 1200-nm- and 1600-nm-thick magnesium-fluoride CTF (Set-up #1).

Columnar thin films of magnesium fluoride were deposited in two different thicknesses, 1200 nm and 1600 nm, to examine the position of reflectance minimum points for both p- and s-polarization of the incident light. A reflectance minimum seen at the same angle independent of the thickness of the CTF is evidence of surface-plasmon-polariton excitation [4]. The excitation of multiple SPP waves has not been recorded for CTFs and has been disproved theoretically [77, 78]. Only one of the reflectance minimums can indicate an SPP wave, but the rest are waveguide modes [4]. If there is an excited SPP wave, this one must be seen for p polarization of the incident light [77, 78]. In this case, the second dip for 1200-nm-thick CTF at $\theta = 51.84°$ and the third dip for 1600-nm-thick CTF at $\theta = 53.01°$ can be considered as indicating an SPP wave, as they are roughly at same angular location.

5.3 Glass-slide/Aluminum/NaF-Chiral-STF Structure

Chiral STFs of sodium fluoride were deposited on 30-nm-thick aluminum films in different periods (3, 4, or 5), each period being 300 nm thick**.** The data were collected for both p and s polarizations of the incident light, using a 45°-90°-45° prism in the Kretschmann configuration (Set-up #1). (For data see Table A.3 in the Appendix).

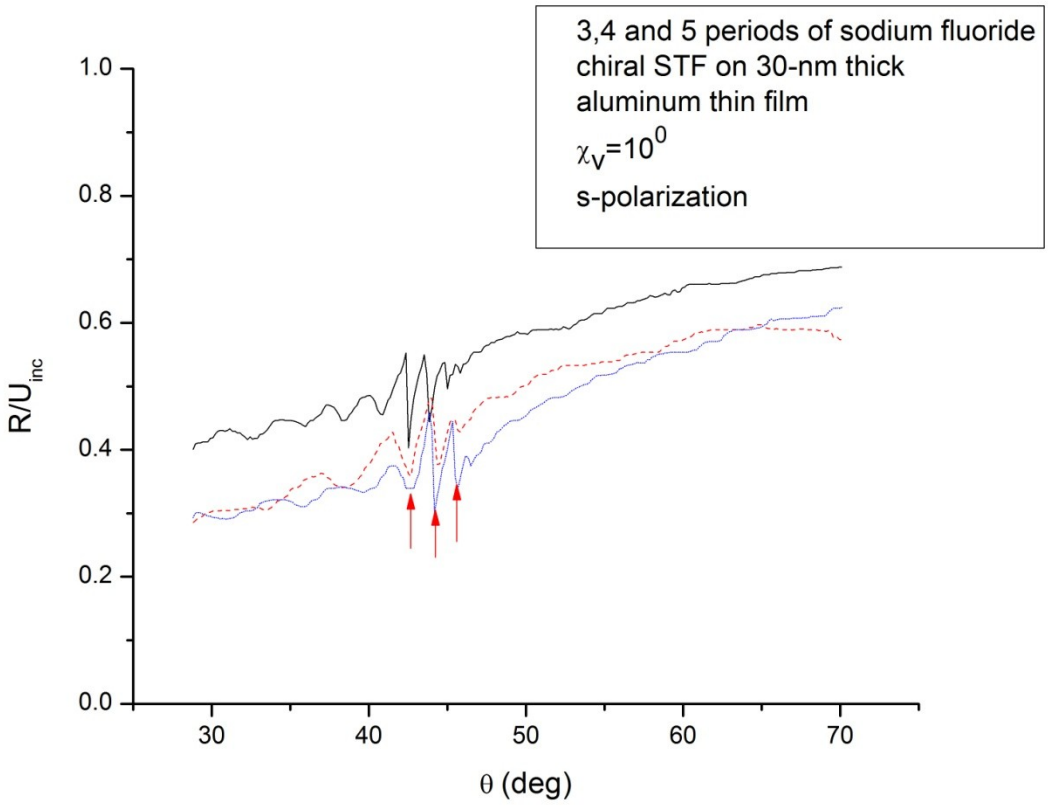

Figure 5.7 Measured reflectance R/U_{inc} as a function of the angle of incidence θ, for a 900-nm-, 1200-nm- and 1500-nm-thick sodium fluoride chiral STF on a 30-nm-thick aluminum film. The incident plane wave is s-polarized and the free-space wavelength is 633 nm. The Kretschmann configuration with a 45°-90°-45° prism was used (Set-up #1).

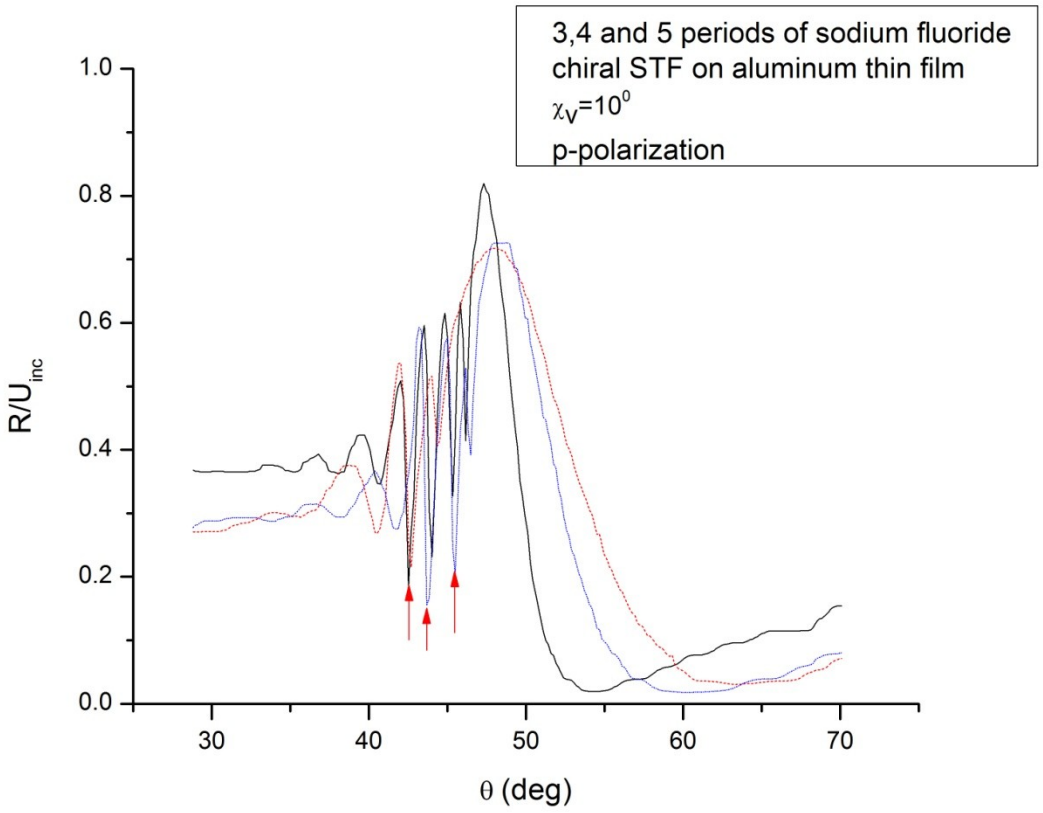

Figure 5.8 Same as Figure 5.7 except that the incident plane wave is p-polarized.

	3periods		4 periods		5 periods	
Polarization of incident light	p	s	p	s	p	s
First dip	40.53°	33.49°	41.65°	35.83°	40.65°	32.59°
Second dip	42.66°	38.41°	43.77°	39.63°	42.54°	35.83°
Third dip	44.34°	42.66°	45.45°	42.54°	44.01°	38.41°
Fourth dip		44.45°	46.47°	44.11°	45.45°	40.76°
Fifth dip		45.80°		45.68°	46.24°	42.54°
Sixth dip				46.47°		43.77°
Seventh dip						45.12°
Eighth dip						45.80°

Table 5.2 Reflectance minimums for 3, 4, and 5 periods of sodium-fluoride chiral STF on aluminum film for both p and s polarization of the incident light (Set-up #1).

The results for the sodium-fluoride chiral STF in Figure 5.7 show that for s polarization of the incident light, there are reflectance minimums for the 3-period-thick chiral STF at $\theta = 33.49°, 38.41°, 42.66°, 44.45°$, and $45.80°$; for the 4-period-thick chiral STF at $\theta = 35.83°, 39.63°, 42.54°, 44.11°, 45.68°$ and $46.47°$; and for the 5-period-thick chiral STF at $\theta = 32.59°, 35.83°, 38.41°, 40.76°, 42.54°, 43.77°, 45.12°$, and $45.80°$. Some of these dips in reflectance may be caused by the waveguide modes excited in the chiral STF, but then their angular locations must depend on the thickness of the chiral STF [4].

There are reflectance minimums that can be considered as independent of the STF thickness. For example, both the first dip of the 4-period-thick chiral STF and the second dip of the 5-period-thick chiral STF are at $\theta = 35.83°$; similarly, both the second dip of the 3-period-thick chiral STF and the third dip of the 5-period-thick chiral STF are at $\theta = 38.41°$. Even though these dips are seen only for two of three different thicknesses of the chiral STF, they can be considered as partial but not conclusive evidence of excitation of multiple SPP waves.

However, the third dips of the 3- and 4-period-thick chiral STFs at $\theta = 42.66°$ and $\theta = 42.54°$, respectively, and the fifth dip of the 5-period-thick chiral STF at $\theta = 42.54°$ indicate the excitation of an SPP wave. Likewise, from the fourth dips of the 3- and 4-period-thick chiral STFs at $\theta = 44.45°$ and $\theta = 44.11°$, respectively, and the sixth dip of the 5-period-thick chiral STF at $\theta = 43.77°$, the excitation of an SPP wave can be inferred. Finally, the fifth dips of 3- and 4-period-thick chiral STF at $\theta = 45.80°$ and $\theta = 45.68°$, respectively, and the eighth dip of the 5-period-thick chiral STF at $\theta = 45.80°$

also imply the excitation of an SPP wave.

For p polarization of the incident light, there are reflectance minimums in Figure 5.8 for the 3-period-thick chiral STF at $\theta = 40.53°$, 42.66°, and 44.34°; for the 4-period-thick chiral STF at $\theta = 41.65°$, 43.77°, 45.45°, and 46.47°; and for the 5-period-thick chiral STF at $\theta = 40.65°$, 42.54°, 44.01°, 45.45°, and 46.24°. Even though there is a slight shift in the angular locations of reflectance minimums of the 4-period-thick chiral STF which may be caused by an experimental error, the first, second and third dips of all three chiral STFs can be considered as independent of the number of periods of the chiral STF, i.e., the thickness of the film, which is good evidence of excitation of three SPP waves.

In conclusion, optical data in Figures 5.7 and 5.8 indicate the launch of up to six different SPP waves, three by incident p-polarized light and three by incident s-polarized light. The experimental observation of multiple SPP waves confirm the theoretical predictions [3, 4] and experimental studies done earlier [6]. The number of different SPP waves is very likely equal to 3, all of which were launched by both p- and s-polarized incident light.

5.4 Glass-slide/Aluminum/ZnSe-Chiral-STF Structure

Chiral STFs of zinc selenide were deposited on aluminum with two different values of the vapor flux angle ($\chi_v = 10°$ and $\chi_v = 15°$). The chiral STFs had different periods (3, 4, and 5), each period being 300 nm. Optical data for zinc-selenide chiral STFs on aluminum were collected with the Kretschmann configuration with hemispherical prism (Set-up #2) and a commercial prism-coupler set-up (Set-up #3). (For data collected by Set-up #2, see Table A.4 in the Appendix).

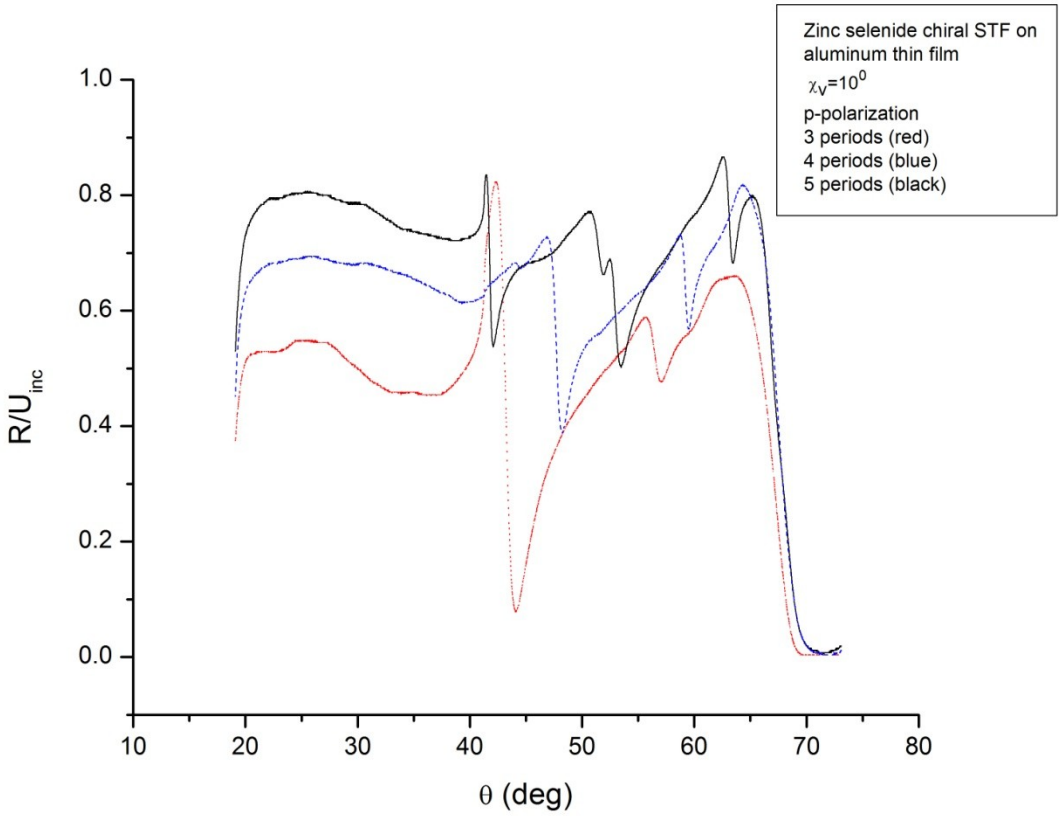

Figure 5.9 Measured reflectance R/U_{inc} as a function of the angle of incidence θ, for a 900-nm-, 1200-nm-, and 1500-nm-thick zinc-selenide chiral STF on a 30-nm-thick aluminum film deposited at $\chi_v = 10°$. The incident plane wave is p-polarized and the free-space wavelength is 633 nm. Commercial prism-coupler set-up (Set-up #3) was used.

	3 periods	4 periods	5 periods
First dip	44.13°	48.20°	42.09°
Second dip	57.13°	59.48°	53.53°
Third dip			63.40°

Table 5.3 Reflectance minimums for 3, 4, and 5 periods of zinc-selenide chiral STF on aluminum film for p polarization of the incident light (Set-up #3).

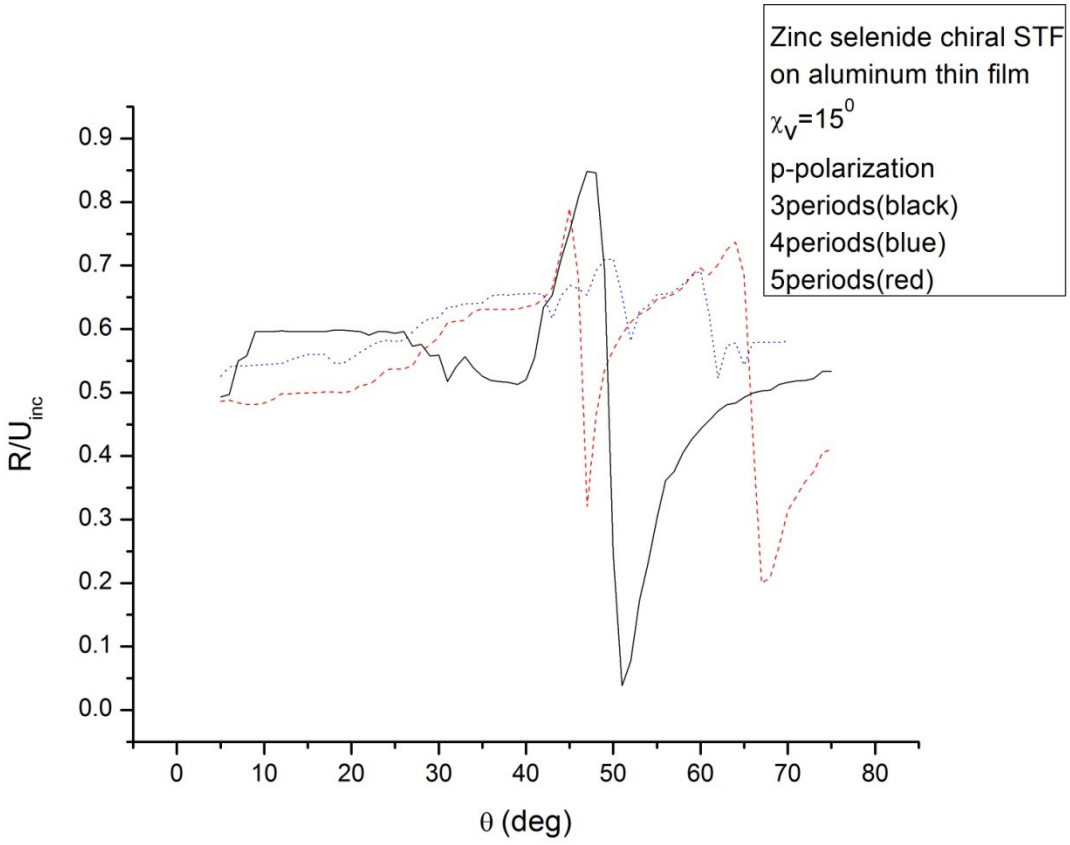

Figure 5.10 Measured reflectance R/U_{inc} as a function of the angle of incidence θ, for a 900-nm-, 1200-nm- and 1500-nm-thick zinc-selenide chiral STF on a 30-nm thick aluminum film. The incident plane wave is p-polarized and the free-space wavelength is 633 nm. The Kretschmann configuration with a hemispherical prism was used (Set-up #2).

	3 periods	4 periods	5 periods
First dip	31.02°	42.91°	46.94°
Second dip	51.18°	51.97°	67.28°
Third dip		62.04°	
Fourth dip		65.07°	

Table 5.4 Reflectance mimimums for 3, 4, and 5 periods of zinc-selenide chiral STF on aluminum film for p polarization of the incident light (Set-up #2).

In order to understand the effect of the angle of incoming vapor flux χ_v, graphs were plotted as before. The data presented in Figure 5.9 and Table 5.3 for the 3-period-thick chiral STF, 4-period-thick chiral STF, and 5-period-thick chiral STF deposited at $\chi_v = 10°$ show no evidence for excitation of SPP waves. But, the results presented in Figure 5.10 and Table 5.4 have shown that the second dip point for the 3-period-thick zinc selenide chiral STF deposited at $\chi_v = 15°$ was at $\theta = 51.18°$ and the second dip point for the 4-period-thick zinc selenide chiral STF at $\theta = 51.97°$. Even though these reflectance minimum points have been seen for only 3- and 4-period-thick chiral STFs and not for the 5-period-thick chiral STF, still it may be only a partial, but not conclusive evidence, of excitation of an SPP wave.

Now, the refractive index of bulk ZnSe is 2.59123. We can estimate that the average refractive index of a 50% porous ZnSe chiral STF as;

$(2.59123 \times 0.5 + 1 \times 0.5) = 1.79562,$

which is greater than the refractive index of BK7 glass. So, the chance of observing an SPP wave is very low. Instead, a high-refractive-index prism with appropriate immersion oil is needed.

5.5 Comparison Of The Results With Previous Experimental Studies

The propagation of multiple SPP waves at the planar interface of a metal and a chiral STF was experimentally observed for the first time by Devender *et al.* [5] in 2009. For this study, 3 or 4 periods of a magnesium-fluoride chiral STF, each period being 425 nm in thickness, were deposited on a 25-nm-thick aluminum film by the thermal evaporation technique. The incoming vapor flux angle for both chiral STFs was fixed at

$\chi_v = 15°$. The reflectance of incident light for different values of the angle of incidence was measured using Kretschmann configuration with a 45°-90°-45° prism (Set-up #1). The experiments were done only for p polarization of incident light. The launch of 2 different SPP waves were observed in this study.

In 2010, Gilani *et al.* [6] conducted another experimental study about excitation of multiple SPP waves. Either 2 or 3 periods of a magnesium-fluoride chiral STF, each period being 400 nm in thickness, were deposited on a 31-nm-thick gold film which had been deposited by sputtering. Both chiral STFs were deposited at $\chi_v = 15°$ by thermal evaporation. The data were collected using Kretschmann configuration (Set-up #1) for both p and s polarizations of incident light. The launch of 4 different SPP waves, 2 for p polarization of incident light and 2 for s polarization of incident light, was observed.

For this thesis, different materials and additional experimental set-ups were used. Also, the chiral STFs 3-, 4- or 5-periods-thick. The incoming vapor flux was not fixed at $\chi_v = 15°$ for all samples. Different values of χ_v was used to deposit both CTFs and chiral STFs. The results for glass-slide/aluminum/NaF-chiral-STF structure indicated the launch of at least 3 different SPP waves. Most importantly, the reflectance minimums for both p and s polarization of incident light were seen at the same angular locations.

CHAPTER 6

Conclusion and Future Work

In this study, the excitation of surface-plasmon-polariton waves guided by the interface of sculptured thin films and metal thin films were examined. For this purpose, chiral sculptured thin films of sodium fluoride and zinc selenide and columnar thin films of magnesium fluoride were deposited on 30-nm-thick aluminum films. By using different experimental set-ups, the reflectance was measured for a range of incidence angles.

The Kretschmann configuration and a commercial prism-coupler set-up were used. In addition, two prisms of different shapes, a 45°-90°-45° prism and a hemispherical prism, were used for the Kretschmann configuration.

The experimental results for Glass-slide/Aluminum structure have shown that there is one reflectance minimum for p polarization of incident light and a quasilinear curve for s polarization of incident light. These results matched well with available data. Results for Glass-slide/Aluminum/MgF_2-CTF structure confirm that multiple SPP waves cannot be excited at the interface of a metal and a CTF. Experiments conducted for Glass Slide/Aluminum/NaF-Chiral-STF structure have shown that there are reflectance minimums independent of the thickness of the chiral STF and these dips indicate the launch of at least 3 different SPP waves.

For the Glass-slide/Aluminum/ZnSe-Chiral-STF structure there is only partial but not conclusive evidence of an SPP wave. The chance of observing SPP waves is very low

because the average refractive index of a ZnSe chiral STF is greater than the refractive index of BK7 glass. A high-refractive-index prism with appropriate immersion oil is needed.

For further research, different materials can be used to deposit both sculptured thin films and metal thin films. Other deposition methods can be used to prepare samples. To ensure the reflectance minimums found are evidence of excited SPP waves but not of the waveguide modes, more experiments should be conducted.

References

1. I. Abdulhalim, M. Zourob, and A. Lakhtakia, "Surface Plasmon Resonance for Biosensing: A Mini-Review," *Electromagnetics* **28**, 214-242 (2008).

2. J. A. Polo, Jr. and A. Lakhtakia, "Surface Electromagnetic Waves: A Review," *Laser Photon. Rev.* **5**, 234-246 (2011).

3. J. A. Polo, Jr. and A. Lakhtakia, "On the Surface Plasmon Polariton Wave at the Planar Interface of a Metal and a Chiral Sculptured Thin Film," *Proc. R. Soc. Lond. A* **465**, 87-107 (2009).

4. M. A. Motyka and A. Lakhtakia, "Multiple Trains of Same-Color Surface Plasmon Polaritons Guided by the Planar Interface of a Metal and a Sculptured Nematic Thin Film," *J. Nanophoton.* **2**, 021910 (2008).

5. Devender, D. P. Pulsifer, and A. Lakhtakia, "Multiple Surface Plasmon Polariton Waves," *Electron. Lett.* **45**, 1137-1138 (2009).

6. T. H. Gilani, N. Duskhkina, W. L. Freeman, M. Z. Numan, D. N. Talwar, and D. P. Pulsifer, "Surface Plasmon Resonance due to the Interface of a Metal and a Chiral Sculptured Thin Film," *Opt. Eng.* **49**, 120503 (2010).

7. A. Lakhtakia, Y.-J. Jen, and C.-F. Lin, "Multiple Trains of Same-Color Surface Plasmon-Polaritons Guided by the Planar Interface of a Metal and a Sculptured Nematic Thin Film. Part III: Experimental Evidence," *J. Nanophoton.* **3**, 033506

(2009).

8. A. Lakhtakia and J. B. Geddes, “Thin-Film Metamaterials Called Sculptured Thin Films,” in *Trends in Nanophysics*, ed. by A. Aldea and V. Bârsan (Springer, Heidelberg, Germany, 2010) pp. 59-71.

9. A. Lakhtakia, R. Messier, M. J. Brett, and K. Robbie, "Sculptured Thin Films (STFs) for Optical, Chemical and Biological Applications,” *Innovations Mater. Res*. **1**, 165-176 (1996).

10. R. Messier, V. C. Venugopal, and P. D. Sunal, “Origin and Evolution of Thin Films,” *J. Vac. Sci. Technol. A* **18**, 1538-1545 (2000).

11. K. Robbie, L. J. Friedrich, S. K. Dew, T. J. Smy, and M. J. Brett, “Fabrication of Thin Films with Highly Porous Microstructures,” *J. Vac. Sci. Technol. A* **13**, 1032-1035 (1995).

12. R. Messier, T. Gehrke, C. Frankel, V. C. Venugopal, W. Otaño, and A. Lakhtakia, “Engineered Sculptured Nematic Thin Films,” *J. Vac. Sci. Technol. A* **15**, 2148-2152 (1997).

13. M. W. McCall, “Combination Morphologies in Sculptured Thin Films,” *Proc. SPIE* **5508**, 77-84 (2004).

14. A. Lakhtakia, M. C. Demirel, M. Horn, and J. Xu, “Six Emerging Directions in Sculptured-Thin-Film Research,” *Adv. Sol. St. Phys.* **46**, 295-307 (2007).

15. V. C. Venugopal, A. Lakhtakia, R. Messier, and J.-P. Kucera, “Low-Permittivity Materials Using Sculptured Thin Film Technology,” *J. Vac. Sci. Technol. B* **18**, 32-36

(2000).

16. F. Zhang, J. Xu, A. Lakhtakia, S. M. Pursel, M. W. Horn, and A. Wang, "Circularly Polarized Emission From Colloidal Nanocrystal Quantum Dots Confined in Cavities Formed by Chiral Mirrors," *Appl. Phys. Lett.* **91**, 023102 (2007).

17. N. O. Young and J. Kowal, "Optically Active Fluorite Films," *Nature* **183**, 104-105 (1959).

18. J. M. Nieuwenhuizen and H. B. Haanstra, "Microfractography of Thin Films," *Phillips Tech. Rev.* **27**, 87-91 (1966).

19. T. Motohiro and Y. Taga, "Thin Film Retardation Plate by Oblique Deposition," *Appl. Opt.* **28**, 2466-2482 (1989).

20. A. Lakhtakia and R. Messier, "The Key to a Thin Film HBM: The Motohiro-Taga Interface," in *Proceedings of Chiral '94; 3rd International Workshop on Chiral, Bi-isotropic and Bianisotropic Media*, ed. by F. Mariotte and J.-P. Parneix (Périgueux, France, 1994) pp. 125-130.

21. K. Robbie, M. J. Brett, and A. Lakhtakia, "First Thin-Film Realization of a Helicoidal Bianisotropic Medium," *J. Vac. Sci. Technol. A* **13**, 2991-2993 (1995).

22. V. C. Venugopal and A. Lakhtakia, "Sculptured Thin Films: Conception, Optical Properties and Applications," in *Electromagnetic Fields in Unconventional Materials and Structures*, ed. by O. N. Singh and A. Lakhtakia (Wiley, New York, NY, USA, 2000) pp. 151-216.

23. A. Lakhtakia and R. Messier, "The Past, the Present, and the Future of Sculptured Thin Films," in *Introduction to Complex Mediums for Optics and Electromagnetics*, ed. by W. S. Weiglhofer and A. Lakhtakia (SPIE Press, Bellingham, WA, USA, 2003) pp. 447-478.

24. J. B. Geddes III, "Towards Shaping of Pulsed Plane Waves in the Time Domain via Chiral Sculptured Thin Films," in *Frontiers in Optical Technology: Materials and Devices*, ed. by P. K. Choudhury and O. N. Singh (Nova Science, Hauppauge, NY, USA, 2006) pp. 1-21.

25. J. A. Polo, "Sculptured Thin Films," in *Micromanufacturing and Nanotechnology*, ed. by N. P. Mahalik (Springer, Berlin, Germany, 2006) pp. 357-381.

26. F. Wang, "Optics of Slanted Chiral STFs," in *Frontiers in Surface Nanophotonics: Principles and Applications,* ed. by D. L. Andrews and Z. Gaburro (Springer, New York, NY, USA, 2007) pp. 129-167.

27. A. Hassani, B. Gauvreau, M. Fehri, A. Kabashin, and M. Skorobogatiy, "Photonic Crystal Fiber and Waveguide-Based Surface Plasmon Resonance Sensors for Application in the Visible and Near-IR," *Electromagnetics* **28**, 198-213 (2008).

28. J. Singh and K. Thyagarajan, "Analysis of Metal Clad Uniaxial Waveguide," *Opt. Commun*. **85**, 397-402 (1991).

29. D. Mihalache, D.-M. Baboiu, M. Ciumac, L. Torner, and J. P. Torres, "Hybrid Surface Plasmon Polaritons Guided by Ultrathin Metal Films," *Opt. Quant. Electron*. **26**, 857-863 (1994).

30. J. Homola, S. S. Yee, and G. Gauglitz, "Surface Plasmon Resonance Sensors: Review," *Sens. Actuat. B: Chem.* **54**, 3-15 (1999).

31. U. Aoki, K. Shimada, M. Nagano, M. Kawai, and H. Koga, "A Novel Approach to Protein Expression Profiling Using Antibody Microarrays Combined with Surface Plasmon Resonance Technology," *Proteomics* **5**, 2396-2401 (2005).

32. V. Kanda, P. Kitov, D. R. Bundle, and M. T. McDermott, "Surface Plasmon Resonance Imaging Measurements of the Inhibition of Shiga-Like Toxin by Synthetic Multivalent Inhibitors," *Anal. Chem*. **77**, 7497-7504 (2005).

33. P. G. de Gennes and J. Prost, *The Physics of Liquid Crystals,* 2nd ed. (Clarendon Press, Oxford, UK, 2003) pp. 271-280.

34. P. W. Baumeister, *Optical Coating Technology* (SPIE Press, Bellingham, WA, USA, 2004) pp. 5-26.

35. M. Faryad and A. Lakhtakia, "On Surface Plasmon-Polariton Waves Guided by the Interface of a Metal and a Rugate Filter with a Sinusoidal Refractive-Index Profile," *J. Opt. Soc. Am. B* **27**, 2218-2223 (2010).

36. M. Faraday, "Experimental Relations of Gold (and other metals) to Light," *Phil. Trans. Roy. Soc. Lond.* **147**, 145-181 (1857).

37. A. Kundt, "Ueber die Electromagnetische Drehung der Polarisationsebene des Lichtes im Eisen," *Ann. Phys. Chem. Lpz.* **27**, 191-202 (1886).

38. H. König and G. Helwig, "Über die Struktur Schräg Aufgedampfter Schichten und ihr Einfluß auf die Entwicklung Submikroskopischer Oberflachenrauhigkeiten," *Optik* **6**, 111-124 (1950).

39. L. Holland, "The Effect of Vapor Incidence on the Structure of Evaporated Aluminum Films," *J. Opt. Soc. Am.* **43**, 376-380 (1953).

40. L. Holland, *Vapor Deposition of Thin Films* (Wiley, New York, NY, USA, 1956).

41. B. A. Movchan and A. V. Demchishin, "Study of the Structure and Properties of Thick Vacuum Condensates of Nickel, Titanium, Tungsten, Aluminum Oxide and Zirconium Dioxide," *Phys. Metal. Metallogr.* **28**, 83-90 (1969).

42. A. Lakhtakia and R. Messier, *Sculptured Thin Films: Nanoengineered Morphology and Optics* (SPIE Press, Bellingham, WA, USA, 2005).

43. A. Hurion, "Variations des Propriétés Physiques du Bismuth Placé dans un Champ Magnétique, *C. R. Acad. Sci. Paris* **98**, 1257-1259 (1884).

44. J. A. Thornton, "High Rate Thick Film Growth," *Annu. Rev. Mater. Sci.* **7**, 239-260 (1977).

45. R. S. Sennett and G. D. Scott, "The Structure of Evaporated Metal Films and Their Optical Properties," *J. Opt. Soc. Am.* **42**, 686-690 (1952).

46. T. M. Donovan and K. Heinemann, "High-Resolution Electron Microscope Observations of Voids in Amorphous Ge," *Phys. Rev. Lett.* **27**, 1794-1796 (1971).

47. S. Nakahara, "Microporosity in Thin Films," *Thin Solid Films* **64**, 149-161 (1979).

48. R. H. Wade and J. Silcox, "Columnar Structure Thin Vacuum-Condensed Pd Films," *Appl. Phys. Lett.* **8**, 7-10 (1966).

49. R. H. Wade and J. Silcox, “Small Angle Electron Scattering From Vacuum Condensed Metallic Films I. Theory,” *Phys. Stat. Sol.* **19**, 57-62 (1967).

50. R. H. Wade and J. Silcox, “Small Angle Electron Scattering From Vacuum Condensed Metallic Films II. Experimental Results,” *Phys. Stat. Sol.* **19**, 63-76 (1967).

51. A. G. Dirks and H. J. Leamy, “Columnar Microstructure in Vapor-Deposited Thin Films,” *Thin Solid Films* **47**, 219-233 (1977).

52. D. Henderson, M. H. Brodsky, and P. Chaudhari, “Simulation of Structural Anisotropy and Void Formation in Amorphous Thin Films,” *Appl. Phys. Lett*. **25**, 641-643 (1980).

53. R. Messier, A. P. Giri, and R. A. Roy, “Revised Structure Zone Model for Thin Film Physical Structure,” *J. Vac. Sci. Technol. A* **2**, 500-503 (1984).

54. R. A. Roy and R. Messier, “Evolutionary Growth Development in SiC Sputtered Films,” *Mater. Res. Soc. Symp. Proc.* **38**, 363-370 (1985).

55. R. Messier, S. V. Krishnaswamy, L. R. Gilbert, and P. Swab, “Black a-Si Solar Selective Absorber Surfaces,” *J. Appl. Phys.* **51**, 1611-1614 (1980).

56. R. Messier and R. C. Ross, “Evolution of Microstructure in Amorphous Hydro-Genated Silicon,” *J. Appl. Phys.* **53**, 6220-6225 (1982).

57. R. A. Roy and R. Messier, “Preparation-Physical Structure Relations in SiC Sputtered Films,” *J. Vac. Sci. Technol. A* **2**, 312-315 (1984).

58. R. Messier and J. E. Yehoda, “Geometry of Thin-Film Morphology,” *J. Appl. Phys.* **58**, 3739-3746 (1985).

59. J. E. Yehoda and R. Messier, "Quantitative Analysis of Thin Film Morphology Evolution," *Proc. SPIE* **678**, 32-40 (1986).

60. J. E. Yehoda, B. Yang, K. Vedam, and R. Messier, "Investigation of the Void Structure in Amorphous Germanium Thin Films as a Function of Low-Energy Ion Bombardment," *J. Vac. Sci. Technol. A* **6**, 1631-1635 (1988).

61. S. V. Krishnaswamy, R. Messier, Y. S. Ng, and T. T. Tsong, "Thin Film Characterization by Atom Probe Field Ion Microscopy," *Appl. Phys. Lett.* **35**, 870-872 (1979).

62. S. V. Krishnaswamy, R. Messier, S. B. McLane, Y. S. Ng, and T. T. Tsong, "Cluster Formation in Amorphous and Polycrystalline Thin Films," *Thin Solid Films* **79**, 21-26 (1981).

63. D. O. Smith, M. S. Cohen, and G. P. Weiss, "Oblique-Incidence Anisotropy in Evaporated Permalloy Films," *J. Appl. Phys.* **31**, 1755-1762 (1960).

64. H. van Kranenburg and C. Lodder, "Tailoring Growth and Local Composition by Oblique-Incidence Deposition: A Review and New Experimental Data," *Mater. Sci. Eng. R* **11**, 295-354 (1994).

65. A. Baltz, "Electron Microscope Study of the Roughness of Permalloy Films Using Surface Replication," *J. Appl. Phys.* **33**, 1115-1116 (1962).

66. T. Motohiro and Y. Taga, "Thin Film Retardation Plate by Oblique Deposition," *Appl. Opt.* **28**, 2466-2482 (1989).

67. A. Kundt, "Üeber Doppelbrechung des Lichtes in Metallschichten, Welche durch Zerstauben einer Kathode Herergestelt Sind," *Ann. Phys. Chem. Lpz*. **27**, 59-71 (1986).

68. K. Robbie, M. J. Brett, and A. Lakhtakia, "Chiral Sculptured Thin Films," *Nature* **384**, 616 (1996).

69. L. I. Maissel and R. Glang, *Handbook of Thin Film Technology* (McGraw-Hill, New York, NY, USA, 1970).

70. S. M. Rossnagel, "Thin Film Deposition with Physical Vapor deposition and Related Technologies," *J. Vac. Sci. Technol. A* **21**, 74-87 (2003).

71. J. C. Sit, D. Vick, K. Robbie, and M. J. Brett, "Thin Film Microstructure Control Using Glancing Angle Deposition by Sputtering," *J. Mater. Res*. **14**, 1197-1199 (1999).

72. D. Vick, Y. Y. Tsui, M. J. Brett, and R. Fedosejevs, "Production of Porous Carbon Thin Films by Pulsed Laser Deposition," *Thin Solid Films* **350**, 49-52 (1999).

73. E. Kretschmann and H. Raether, "Radiative Decay of Nonradiative Surface Plasmons Excited by Light," *Z. Naturforsch. A* **23**, 2135-2136 (1968).

74. Retrieved from http://www.refractiveindex.info/ on June 25, 2011.

75. H. J. Simon, D. E. Mitchell, and J. G. Watson, "Surface Plasmons in Silver Films-A Novel Undergraduate Experiment," *Am. J. Phys*. **43**, 630-636 (1975).

76. M. Mansuripur and L. Li, "What in The World Are Surface Plasmons," *Opt. Photon. News* **8 (5)**, 50-55 (1997 May issue).

77. A. Lakhtakia and J. A. Polo, Jr., "Morphological Influence on Surface-Wave Propagation at The Planar Interface of A Metal Film and A Columnar Thin Film," *Asian J. Phys*. **17**, 185-191 (2008).

78. J. A. Polo, Jr. and A. Lakhtakia, "Morphological Effects on Surface-Plasmon-Polariton Waves at the Planar Interface of A Metal and A Columnar Thin Film," *Opt. Commun*. **281**, 5453-5457 (2008).

Appendix A: Selected Optical Data

Table A.1 Optical data for glass-slide/aluminum structure (Set-up #1).

Al			
Polarization of incident light		p	s
Φ(deg)	θ(deg)	R/U_{inc}	R/U_{inc}
-8	39.7295	0.42946	0.48214
-7.8	39.86079	0.4375	0.48393
-7.6	39.99212	0.44196	0.48214
-7.4	40.12348	0.46518	0.48214
-7.2	40.25488	0.48393	0.48482
-7	40.38631	0.51696	0.49375
-6.8	40.51778	0.55357	0.49911
-6.6	40.64927	0.6375	0.49911
-6.4	40.7808	0.82232	0.50089
-6.2	40.91235	0.84375	0.5
-6	41.04393	0.82321	0.50089
-5.8	41.17554	0.78571	0.52143
-5.6	41.30718	0.74375	0.525
-5.4	41.43884	0.67143	0.53571
-5.2	41.57052	0.60714	0.54286
-5	41.70223	0.53571	0.54554
-4.8	41.83396	0.45893	0.54821
-4.6	41.96572	0.39375	0.55268
-4.4	42.09749	0.32768	0.55089
-4.2	42.22929	0.26696	0.55268
-4	42.3611	0.21518	0.55357
-3.8	42.49294	0.17857	0.55357
-3.6	42.62479	0.14196	0.55446
-3.4	42.75665	0.10714	0.55357
-3.2	42.88853	0.08866	0.55536
-3	43.02043	0.07116	0.55893
-2.8	43.15234	0.05571	0.55893
-2.6	43.28426	0.04116	0.56161
-2.4	43.4162	0.03571	0.5625
-2.2	43.54814	0.03063	0.56964
-2	43.6801	0.02125	0.57143
-1.8	43.81206	0.01812	0.57321

-1.6	43.94403	0.01723	0.57768
-1.4	44.07601	0.01625	0.57946
-1.2	44.208	0.01696	0.57857
-1	44.33999	0.01741	0.58571
-0.8	44.47199	0.0183	0.5875
-0.6	44.60399	0.01991	0.58929
-0.4	44.73599	0.02179	0.58929
-0.2	44.86799	0.02411	0.58929
0	45	0.02661	0.58929
0.2	45.13201	0.03134	0.58929
0.4	45.26401	0.03491	0.58929
0.6	45.39601	0.03563	0.58839
0.8	45.52801	0.03598	0.58929
1	45.66001	0.03723	0.59107
1.2	45.792	0.04205	0.59554
1.4	45.92399	0.04875	0.59375
1.6	46.05597	0.05321	0.60446
1.8	46.18794	0.05464	0.60446
2	46.3199	0.05857	0.60357
2.2	46.45186	0.06429	0.60357
2.4	46.5838	0.06991	0.60893
2.6	46.71574	0.07134	0.60982
2.8	46.84766	0.07161	0.60893
3	46.97957	0.07312	0.61696
3.2	47.11147	0.07411	0.61607
3.4	47.24335	0.07866	0.61875
3.6	47.37521	0.08473	0.61964
3.8	47.50706	0.08777	0.62143
4	47.6389	0.08929	0.61964
4.2	47.77071	0.08929	0.62411
4.4	47.90251	0.09107	0.62411
4.6	48.03428	0.09375	0.62411
4.8	48.16604	0.09911	0.625
5	48.29777	0.10536	0.625
5.2	48.42948	0.10625	0.62411
5.4	48.56116	0.10714	0.625
5.6	48.69282	0.10714	0.625
5.8	48.82446	0.10804	0.62589
6	48.95607	0.11071	0.625
6.2	49.08765	0.11429	0.62589
6.4	49.2192	0.11607	0.62589
6.6	49.35073	0.12143	0.62857
6.8	49.48222	0.125	0.62946
7	49.61369	0.12589	0.62946

7.2	49.74512	0.12768	0.63929
7.4	49.87652	0.12946	0.63661
7.6	50.00788	0.13393	0.64018
7.8	50.13921	0.13661	0.64196
8	50.2705	0.13839	0.64286
8.2	50.40176	0.14286	0.64107
8.4	50.53298	0.14286	0.64286
8.6	50.66416	0.14286	0.64375
8.8	50.7953	0.14286	0.64464
9	50.92641	0.14375	0.64911

Table A.2 Optical data for glass-slide/aluminum/MgF_2 CTF structure (Set-up #1).

MgF_2 CTF					
Thickness of CTF		1200 nm		1600 nm	
Polarization of incident light		p	s	p	s
Φ(deg)	θ(deg)	R/U_{inc}	R/U_{inc}	R/U_{inc}	R/U_{inc}
-4	42.3611	0.39196	0.13393	0.43214	0.57143
-3.8	42.49294	0.41071	0.14286	0.44732	0.53571
-3.6	42.62479	0.43036	0.17679	0.46339	0.48482
-3.4	42.75665	0.46161	0.20179	0.52232	0.41071
-3.2	42.88853	0.48214	0.23214	0.55268	0.32143
-3	43.02043	0.51696	0.25	0.57321	0.32321
-2.8	43.15234	0.53393	0.25804	0.59018	0.41071
-2.6	43.28426	0.55357	0.28036	0.62321	0.45446
-2.4	43.4162	0.58839	0.30268	0.64554	0.49107
-2.2	43.54814	0.6125	0.30982	0.66161	0.5
-2	43.6801	0.64554	0.32321	0.69554	0.51964
-1.8	43.81206	0.67589	0.33571	0.73393	0.53661
-1.6	43.94403	0.70357	0.34018	0.74821	0.55357
-1.4	44.07601	0.73214	0.35089	0.78482	0.56696
-1.2	44.208	0.7625	0.36339	0.79286	0.57143
-1	44.33999	0.79821	0.37411	0.76607	0.57143
-0.8	44.47199	0.81696	0.37589	0.625	0.575
-0.6	44.60399	0.82232	0.38125	0.375	0.58929
-0.4	44.73599	0.83036	0.39196	0.10893	0.58929
-0.2	44.86799	0.80446	0.39286	0.02911	0.59911
0	45	0.75982	0.39464	0.03679	0.60357
0.2	45.13201	0.69643	0.40804	0.08929	0.60714
0.4	45.26401	0.55714	0.41071	0.13929	0.60804
0.6	45.39601	0.43393	0.41161	0.14286	0.62143
0.8	45.52801	0.30357	0.41339	0.19732	0.62054
1	45.66001	0.17946	0.42321	0.24911	0.62321
1.2	45.792	0.12857	0.42768	0.27857	0.6375
1.4	45.92399	0.06652	0.43125	0.32054	0.64554
1.6	46.05597	0.02857	0.44286	0.34821	0.65089
1.8	46.18794	0.01446	0.44643	0.37589	0.67411
2	46.3199	0.0175	0.45	0.40268	0.67857
2.2	46.45186	0.03554	0.45089	0.42411	0.68929
2.4	46.5838	0.06062	0.46339	0.44643	0.71518
2.6	46.71574	0.0892	0.47679	0.46518	0.74554
2.8	46.84766	0.10804	0.48214	0.48304	0.76786
3	46.97957	0.14643	0.49375	0.50982	0.82143

3.2	47.11147	0.18214	0.50625	0.51786	0.88839
3.4	47.24335	0.21429	0.52143	0.54018	0.56696
3.6	47.37521	0.25	0.54107	0.55714	0.23125
3.8	47.50706	0.28482	0.56875	0.58661	0.37143
4	47.6389	0.32143	0.6	0.60357	0.43214
4.2	47.77071	0.35625	0.64286	0.625	0.48214
4.4	47.90251	0.39286	0.71786	0.64107	0.51696
4.6	48.03428	0.425	0.82857	0.66071	0.53661
4.8	48.16604	0.44643	0.875	0.69643	0.55357
5	48.29777	0.48214	0.25179	0.71964	0.57054
5.2	48.42948	0.51786	0.17857	0.74643	0.58482
5.4	48.56116	0.55357	0.23393	0.7625	0.58393
5.6	48.69282	0.57321	0.28393	0.78929	0.58929
5.8	48.82446	0.61518	0.30804	0.79643	0.60625
6	48.95607	0.64107	0.31786	0.7875	0.60714
6.2	49.08765	0.65714	0.33661	0.78571	0.61339
6.4	49.2192	0.68661	0.34196	0.73214	0.61339
6.6	49.35073	0.69643	0.35625	0.51875	0.61607
6.8	49.48222	0.7125	0.36696	0.21429	0.62411
7	49.61369	0.72857	0.375	0.17679	0.63036
7.2	49.74512	0.75089	0.37679	0.0217	0.63304
7.4	49.87652	0.76607	0.39196	0.0525	0.63839
7.6	50.00788	0.78304	0.39911	0.12054	0.64821
7.8	50.13921	0.78571	0.41071	0.21429	0.65268
8	50.2705	0.79911	0.41339	0.25179	0.65982
8.2	50.40176	0.80268	0.42589	0.35536	0.67857
8.4	50.53298	0.81071	0.43036	0.41071	0.67857
8.6	50.66416	0.81339	0.44107	0.44643	0.71964
8.8	50.7953	0.80357	0.44554	0.48214	0.77679
9	50.92641	0.78571	0.44643	0.54643	0.83839
9.2	51.05746	0.7125	0.44732	0.55714	0.29286
9.4	51.18848	0.62768	0.45357	0.58929	0.41071
9.6	51.31946	0.51786	0.46071	0.62411	0.50625
9.8	51.45039	0.375	0.4625	0.65982	0.55446
10	51.58127	0.21429	0.46518	0.68571	0.57321
10.2	51.71211	0.07429	0.46875	0.69643	0.60536
10.4	51.8429	0.02518	0.475	0.72946	0.61161
10.6	51.97365	0.03598	0.48125	0.76607	0.62411
10.8	52.10434	0.14464	0.48304	0.78393	0.62589
11	52.23499	0.26696	0.49554	0.80714	0.64018
11.2	52.36558	0.39286	0.51518	0.80446	0.64196
11.4	52.49613	0.50804	0.53393	0.8	0.64286

11.6	52.62662	0.60446	0.56786	0.74732	0.64375
11.8	52.75705	0.66161	0.69107	0.53482	0.64732
12	52.88743	0.72054	0.29732	0.08929	0.65
12.2	53.01776	0.76339	0.35804	0.02554	0.64375
12.4	53.14803	0.7875	0.39464	0.08911	0.64375
12.6	53.27824	0.79375	0.42143	0.24732	0.65982
12.8	53.40839	0.79554	0.44732	0.34107	0.66339
13	53.53849	0.78661	0.46071	0.44643	0.67679
13.2	53.66852	0.78036	0.46607	0.60446	0.69464
13.4	53.79849	0.75268	0.47857	0.67143	0.72143
13.6	53.9284	0.73304	0.48214	0.7625	0.47054
13.8	54.05825	0.70268	0.48214	0.78661	0.60804
14	54.18803	0.68125	0.48304	0.80268	0.64107
14.2	54.31774	0.65536	0.48393	0.82232	0.64375
14.4	54.44739	0.62321	0.49018	0.825	0.65
14.6	54.57698	0.59286	0.49286	0.82143	0.66339
14.8	54.70649	0.56696	0.49821	0.79107	0.66875
15	54.83594	0.55357	0.5	0.76607	0.67232
15.2	54.96531	0.54196	0.5	0.75	0.67589
15.4	55.09461	0.51786	0.5	0.69643	0.67857
15.6	55.22384	0.48393	0.5	0.66607	0.67857
15.8	55.353	0.4625	0.50089	0.625	0.67857
16	55.48208	0.44464	0.50089	0.57321	0.68125
16.2	55.61109	0.41161	0.50268	0.52232	0.67857
16.4	55.74002	0.39464	0.50357	0.48393	0.68036
16.6	55.86887	0.375	0.50536	0.42946	0.67946
16.8	55.99765	0.35714	0.50804	0.38125	0.67946
17	56.12635	0.34196	0.51071	0.33929	0.68036
17.2	56.25496	0.33214	0.51339	0.3	0.67857
17.4	56.38349	0.30536	0.51696	0.25089	0.68482
17.6	56.51195	0.28929	0.51696	0.23214	0.67857
17.8	56.64031	0.28214	0.51786	0.19732	0.68304
18	56.7686	0.25804	0.51786	0.16964	0.68214
18.2	56.89679	0.25	0.51786	0.16429	0.68304
18.4	57.0249	0.23393	0.51786	0.14107	0.67946
18.6	57.15293	0.21696	0.51786	0.12411	0.67857
18.8	57.28086	0.20893	0.51786	0.10357	0.68929
19	57.4087	0.19554	0.51786	0.08884	0.69375
19.2	57.53646	0.18036	0.51875	0.07223	0.68571
19.4	57.66412	0.17679	0.51964	0.06518	0.67857
19.6	57.79169	0.16161	0.52232	0.05429	0.68839
19.8	57.91916	0.15	0.52054	0.04259	0.68929

20	58.04654	0.14286	0.52232	0.03589	0.67857
20.2	58.17382	0.13571	0.52411	0.03554	0.69821
20.4	58.30101	0.12589	0.52589	0.03348	0.69911
20.6	58.4281	0.11696	0.53036	0.02732	0.69464
20.8	58.55509	0.10893	0.53125	0.02286	0.70268
21	58.68197	0.10714	0.53304	0.02	0.69732
21.2	58.80876	0.10446	0.53393	0.01902	0.69732
21.4	58.93544	0.09554	0.53482	0.01848	0.69911
21.6	59.06202	0.09018	0.53482	0.01839	0.70179
21.8	59.1885	0.08929	0.53571	0.01866	0.70625
22	59.31486	0.08884	0.53661	0.01911	0.70089
22.2	59.44113	0.08589	0.53661	0.02027	0.69821
22.4	59.56728	0.08062	0.53661	0.0217	0.69464
22.6	59.69332	0.075	0.5375	0.0242	0.68571
22.8	59.81926	0.07295	0.5375	0.02786	0.70268
23	59.94508	0.07179	0.53839	0.03125	0.70536
23.2	60.07079	0.07143	0.53929	0.02991	0.69643
23.4	60.19638	0.07116	0.54107	0.03241	0.69643
23.6	60.32186	0.07018	0.54018	0.03438	0.69732
23.8	60.44723	0.06866	0.54286	0.03545	0.70536
24	60.57247	0.06563	0.54375	0.03571	0.70446
24.2	60.6976	0.06241	0.54464	0.03598	0.70714
24.4	60.82261	0.05973	0.54375	0.03696	0.70714
24.6	60.9475	0.05741	0.54643	0.03955	0.70893
24.8	61.07227	0.05607	0.54732	0.04455	0.71161
25	61.19691	0.05527	0.54911	0.04893	0.71429
25.2	61.32143	0.05464	0.55089	0.05143	0.71518
25.4	61.44583	0.05411	0.55179	0.05375	0.71429
25.6	61.5701	0.05375	0.55179	0.05554	0.71429
25.8	61.69424	0.0542	0.55357	0.05938	0.71429
26	61.81825	0.0542	0.55357	0.06464	0.71964
26.2	61.94213	0.05366	0.55357	0.06848	0.72232
26.4	62.06588	0.05366	0.55357	0.07071	0.72232
26.6	62.1895	0.05295	0.55357	0.07143	0.72679
26.8	62.31299	0.05286	0.55357	0.07161	0.72321
27	62.43634	0.05268	0.55357	0.07196	0.71429
27.2	62.55955	0.05232	0.55357	0.07482	0.71429
27.4	62.68263	0.05232	0.55357	0.07929	0.71429
27.6	62.80557	0.0525	0.55357	0.08188	0.71429
27.8	62.92837	0.05268	0.55357	0.08688	0.71429
28	63.05102	0.05268	0.55357	0.08848	0.71518
28.2	63.17354	0.05286	0.55357	0.08866	0.71607

28.4	63.29591	0.05304	0.55357	0.08911	0.71429
28.6	63.41814	0.05312	0.55357	0.08929	0.72054
28.8	63.54022	0.05357	0.55357	0.09107	0.71518
29	63.66216	0.05357	0.55357	0.09464	0.72232
29.2	63.78395	0.05366	0.55357	0.09732	0.71518
29.4	63.90558	0.05393	0.55357	0.10357	0.71607
29.6	64.02707	0.0542	0.55357	0.10536	0.71696
29.8	64.14841	0.055	0.55357	0.10714	0.72143
30	64.26959	0.05554	0.55357	0.10714	0.71964
30.2	64.39062	0.05652	0.55357	0.10714	0.72857
30.4	64.51149	0.05741	0.55357	0.10804	0.72768
30.6	64.6322	0.05866	0.55446	0.11071	0.72589
30.8	64.75276	0.06009	0.55357	0.11607	0.72946
31	64.87315	0.05902	0.55446	0.11875	0.72679
31.2	64.99339	0.06089	0.55446	0.12143	0.73125
31.4	65.11346	0.06187	0.55446	0.125	0.73125
31.6	65.23337	0.06438	0.55536	0.125	0.73125
31.8	65.35311	0.06625	0.55357	0.12768	0.73214
32	65.47269	0.06759	0.55446	0.13036	0.73214
32.2	65.5921	0.06866	0.55446	0.13482	0.73304
32.4	65.71134	0.06982	0.55446	0.13839	0.73214
32.6	65.83041	0.07063	0.55446	0.14018	0.73214
32.8	65.94931	0.07107	0.55357	0.14018	0.73393
33	66.06804	0.07125	0.55446	0.14196	0.73482
33.2	66.18659	0.07143	0.55357	0.14286	0.73304
33.4	66.30497	0.07161	0.55357	0.14286	0.73304
33.6	66.42317	0.0717	0.55357	0.14286	0.73125
33.8	66.54119	0.07205	0.55446	0.14286	0.73214
34	66.65903	0.07232	0.55357	0.14286	0.73304
34.2	66.77669	0.0733	0.55446	0.14375	0.73482
34.4	66.89417	0.07518	0.55357	0.14464	0.73214
34.6	67.01146	0.07634	0.55357	0.14911	0.73214
34.8	67.12857	0.07768	0.55357	0.15179	0.73304
35	67.24549	0.0808	0.55357	0.15179	0.73214
35.2	67.36223	0.08152	0.55357	0.15714	0.73393
35.4	67.47877	0.08223	0.55357	0.15804	0.73482
35.6	67.59512	0.085	0.55357	0.15893	0.73571
35.8	67.71129	0.08571	0.55357	0.16071	0.73929
36	67.82725	0.08679	0.55357	0.15982	0.73482
36.2	67.94302	0.08723	0.55446	0.16071	0.73839
36.4	68.0586	0.08714	0.55446	0.15982	0.73929
36.6	68.17398	0.08607	0.55357	0.16161	0.73929

36.8	68.28915	0.085	0.55357	0.16429	0.73661
37	68.40413	0.08339	0.55357	0.16429	0.74018
37.2	68.5189	0.08062	0.55357	0.16696	0.73661
37.4	68.63347	0.07696	0.55357	0.17143	0.73482
37.6	68.74784	0.07366	0.55357	0.17054	0.73393
37.8	68.862	0.07205	0.55357	0.17411	0.73482
38	68.97595	0.07152	0.55179	0.17321	0.73482
38.2	69.08968	0.07125	0.54554	0.17232	0.73393
38.4	69.20321	0.06937	0.54018	0.17054	0.73393
38.6	69.31653	0.065	0.53482	0.17232	0.73839
38.8	69.42963	0.05759	0.52411	0.16875	0.73393
39	69.54251	0.05366	0.51786	0.16964	0.73393
39.2	69.65518	0.05205	0.50268	0.16786	0.73571
39.4	69.76763	0.04652	0.49018	0.16518	0.73839
39.6	69.87986	0.04036	0.48036	0.16071	0.73482
39.8	69.99186	0.03679	0.45446	0.16161	0.73393
40	70.10365	--	0.44643	0.16161	0.73482

Table A.3 Optical data for glass-slide/aluminum/NaF-chiral-STF structure (Set-up #1).

NaF chiral STF							
Thickness of chiral STF		3 periods	4 periods	5 periods	3 periods	4 periods	5 periods
Polarization of incident light		p			s		
Φ(deg)	θ (deg)	R/U_{inc}	R/U_{inc}	R/U_{inc}	R/U_{inc}	R/U_{inc}	R/U_{inc}
-25	28.80309	0.27054	0.27745	0.36827	0.28571	0.29286	0.40089
-24.75	28.95891	0.27054	0.28137	0.36635	0.28839	0.30089	0.40893
-24.5	29.11493	0.27054	0.28235	0.36635	0.29196	0.30089	0.41071
-24.25	29.27113	0.27054	0.28529	0.36538	0.29464	0.30089	0.41071
-24	29.42753	0.27143	0.28725	0.36538	0.29554	0.29821	0.4125
-23.75	29.5841	0.27143	0.28824	0.36538	0.3	0.29821	0.4125
-23.5	29.74086	0.27143	0.28824	0.36538	0.30089	0.29554	0.4125
-23.25	29.8978	0.27143	0.28824	0.36538	0.30179	0.29554	0.41786
-23	30.05492	0.27143	0.28824	0.36635	0.30357	0.29375	0.41875
-22.75	30.21222	0.27143	0.28824	0.36635	0.30357	0.29286	0.425
-22.5	30.36969	0.27143	0.28824	0.36635	0.30357	0.29286	0.42857
-22.25	30.52733	0.27143	0.28824	0.36635	0.30357	0.29107	0.43036
-22	30.68514	0.27321	0.28922	0.36635	0.30446	0.29196	0.43036
-21.75	30.84311	0.27321	0.29118	0.36538	0.30446	0.29107	0.42946
-21.5	31.00126	0.275	0.29216	0.36538	0.30446	0.29107	0.43036
-21.25	31.15956	0.27768	0.29216	0.36538	0.30446	0.29196	0.43304
-21	31.31803	0.28036	0.29314	0.36538	0.30536	0.29286	0.42946
-20.75	31.47665	0.28214	0.29314	0.36538	0.30625	0.29375	0.42946
-20.5	31.63543	0.28214	0.29314	0.36538	0.30625	0.29732	0.42679
-20.25	31.79437	0.28393	0.29314	0.36538	0.30625	0.30089	0.42679
-20	31.95346	0.28393	0.29314	0.36538	0.30714	0.30179	0.42321
-19.75	32.1127	0.28482	0.29314	0.36538	0.30714	0.30357	0.42054
-19.5	32.27208	0.28482	0.29314	0.36538	0.30714	0.30357	0.41607
-19.25	32.43162	0.28661	0.29314	0.36635	0.30804	0.30357	0.42054
-19	32.5913	0.28839	0.29314	0.36635	0.30982	0.30446	0.41696
-18.75	32.75111	0.29018	0.29314	0.36635	0.30893	0.30625	0.41786
-18.5	32.91107	0.29107	0.29314	0.36827	0.31071	0.30893	0.41786
-18.25	33.07117	0.29375	0.29118	0.36923	0.30804	0.31607	0.42411
-18	33.2314	0.29643	0.28922	0.37596	0.30625	0.31696	0.425
-17.75	33.39177	0.29821	0.28922	0.37596	0.30536	0.31875	0.42768
-17.5	33.55227	0.3	0.28824	0.37596	0.30536	0.31964	0.43214
-17.25	33.7129	0.30089	0.28725	0.37596	0.30804	0.32054	0.43839

-17	33.87365	0.30089	0.28725	0.37596	0.31071	0.32143	0.44375
-16.75	34.03454	0.30089	0.28725	0.375	0.31429	0.32143	0.44643
-16.5	34.19554	0.30089	0.2902	0.375	0.31964	0.32143	0.44643
-16.25	34.35667	0.3	0.29118	0.37308	0.32054	0.32143	0.44732
-16	34.51792	0.29911	0.29216	0.37115	0.32232	0.32143	0.44732
-15.75	34.67928	0.29911	0.29412	0.36731	0.32589	0.32143	0.44643
-15.5	34.84076	0.29732	0.29412	0.36731	0.32857	0.31964	0.44643
-15.25	35.00236	0.29554	0.2951	0.36635	0.3375	0.31875	0.44643
-15	35.16406	0.29464	0.29608	0.36538	0.33929	0.31696	0.44554
-14.75	35.32588	0.29554	0.3	0.36538	0.33929	0.31339	0.44464
-14.5	35.48781	0.29554	0.30392	0.36635	0.34107	0.3125	0.44286
-14.25	35.64984	0.29375	0.30882	0.36923	0.34375	0.31071	0.44107
-14	35.81197	0.29643	0.31275	0.37981	0.35179	0.31071	0.43839
-13.75	35.97421	0.29732	0.31373	0.38077	0.35357	0.31071	0.43661
-13.5	36.13655	0.30179	0.31373	0.38269	0.35536	0.31339	0.44286
-13.25	36.29898	0.30357	0.31471	0.38654	0.35804	0.31875	0.44643
-13	36.46151	0.30357	0.31373	0.3875	0.35714	0.32054	0.44643
-12.75	36.62414	0.30536	0.31471	0.39038	0.35804	0.32143	0.45089
-12.5	36.78686	0.30982	0.31373	0.39327	0.35982	0.32321	0.45357
-12.25	36.94967	0.31875	0.31275	0.3875	0.36339	0.32857	0.45625
-12	37.11257	0.32411	0.31078	0.38269	0.3625	0.33393	0.46429
-11.75	37.27555	0.33571	0.30686	0.37981	0.35625	0.33839	0.47054
-11.5	37.43862	0.33929	0.30294	0.36731	0.35536	0.33929	0.47054
-11.25	37.60178	0.34018	0.3	0.36538	0.35268	0.33929	0.46875
-11	37.76501	0.35179	0.29608	0.36538	0.34554	0.33929	0.46696
-10.75	37.92833	0.35804	0.29412	0.36346	0.34375	0.34018	0.46161
-10.5	38.09172	0.36429	0.29412	0.3625	0.34196	0.34107	0.45536
-10.25	38.25519	0.37232	0.29412	0.36538	0.34018	0.34196	0.44643
-10	38.41873	0.375	0.29412	0.36538	0.34107	0.34107	0.44643
-9.75	38.58234	0.375	0.29706	0.37885	0.34107	0.34018	0.44732
-9.5	38.74602	0.37589	0.3049	0.39423	0.34286	0.33929	0.45446
-9.25	38.90978	0.375	0.3098	0.40385	0.34464	0.33929	0.45893
-9	39.07359	0.375	0.31373	0.40769	0.34732	0.3375	0.46518
-8.75	39.23748	0.37232	0.32255	0.42212	0.35179	0.33571	0.47054
-8.5	39.40142	0.35893	0.33235	0.42308	0.35625	0.33482	0.47946
-8.25	39.56543	0.35357	0.33431	0.42308	0.36071	0.33304	0.48214
-8	39.7295	0.3375	0.34412	0.42308	0.37054	0.33304	0.48304
-7.75	39.89362	0.32054	0.34706	0.41346	0.375	0.33571	0.48482
-7.5	40.0578	0.30357	0.35588	0.4	0.37768	0.33839	0.48571

-7.25	40.22203	0.29107	0.36078	0.37788	0.38482	0.33929	0.48214
-7	40.38631	0.26964	0.36667	0.35865	0.39286	0.34018	0.47589
-6.75	40.55065	0.26875	0.36078	0.34712	0.4	0.34375	0.46339
-6.5	40.71503	0.27768	0.35294	0.34615	0.40982	0.35446	0.45625
-6.25	40.87946	0.29732	0.3402	0.35865	0.41071	0.35893	0.45536
-6	41.04393	0.31518	0.33235	0.38077	0.41518	0.3625	0.46518
-5.75	41.20845	0.38929	0.31176	0.40385	0.41786	0.37232	0.47768
-5.5	41.373	0.43125	0.29412	0.42692	0.425	0.375	0.48304
-5.25	41.5376	0.47589	0.27745	0.44712	0.42768	0.375	0.49643
-5	41.70223	0.50625	0.27549	0.48077	0.41071	0.375	0.50625
-4.75	41.8669	0.53571	0.27549	0.49904	0.40893	0.37054	0.51696
-4.5	42.0316	0.53661	0.29216	0.50865	0.39286	0.35982	0.52143
-4.25	42.19634	0.48482	0.30196	0.47885	0.38125	0.35536	0.53571
-4	42.3611	0.41875	0.33725	0.32981	0.37411	0.33929	0.55268
-3.75	42.5259	0.25268	0.36078	0.18269	0.36161	0.33929	0.40268
-3.5	42.69072	0.21518	0.39608	0.27019	0.35893	0.33929	0.44911
-3.25	42.85556	0.27054	0.44608	0.32404	0.38571	0.33929	0.48214
-3	43.02043	0.3375	0.56863	0.44904	0.40893	0.35268	0.50089
-2.75	43.18532	0.375	0.59314	0.51923	0.42143	0.3625	0.51786
-2.5	43.35023	0.40804	0.58824	0.56923	0.43304	0.39107	0.52946
-2.25	43.51516	0.44643	0.41176	0.59615	0.44643	0.40536	0.55
-2	43.6801	0.48393	0.1549	0.5375	0.46339	0.43393	0.51964
-1.75	43.84505	0.51071	0.16667	0.30481	0.48125	0.45893	0.44375
-1.5	44.01002	0.51607	0.25196	0.23173	0.48125	0.42946	0.46786
-1.25	44.175	0.46429	0.33333	0.32788	0.42857	0.30089	0.49821
-1	44.33999	0.40536	0.41373	0.44423	0.37679	0.32679	0.51607
-0.75	44.50499	0.41518	0.46275	0.52692	0.37768	0.34643	0.52411
-0.5	44.66999	0.46161	0.52941	0.59615	0.39554	0.37143	0.53571
-0.25	44.83499	0.49643	0.56863	0.61538	0.41071	0.38214	0.5375
0	45	0.53571	0.57647	0.57692	0.42768	0.40268	0.49554
0.25	45.16501	0.5625	0.5049	0.4375	0.44375	0.425	0.51696
0.5	45.33001	0.58929	0.24804	0.32692	0.44732	0.44464	0.51875
0.75	45.49501	0.60446	0.2049	0.42308	0.44643	0.35625	0.53482
1	45.66001	0.61339	0.32745	0.57692	0.43036	0.33929	0.53125
1.25	45.825	0.625	0.43039	0.63269	0.42768	0.35536	0.52054
1.5	45.98998	0.64196	0.47941	0.57308	0.43661	0.37589	0.53482
1.75	46.15495	0.65536	0.52843	0.41442	0.44286	0.39018	0.53571
2	46.3199	0.6625	0.43137	0.53558	0.44643	0.3875	0.53929
2.25	46.48484	0.675	0.39118	0.65288	0.44821	0.375	0.54821

2.5	46.64977	0.67946	0.4902	0.71058	0.46071	0.38214	0.55357
2.75	46.81468	0.69464	0.54902	0.73077	0.46518	0.39018	0.55357
3	46.97957	0.69643	0.62843	0.77212	0.46786	0.39286	0.55357
3.25	47.14444	0.69911	0.64706	0.80673	0.47232	0.39643	0.55446
3.5	47.30928	0.70804	0.67157	0.81923	0.47768	0.40893	0.56161
3.75	47.4741	0.71161	0.68824	0.80769	0.48125	0.41071	0.56429
4	47.6389	0.71518	0.70686	0.80192	0.48125	0.41071	0.56518
4.25	47.80366	0.71696	0.72255	0.77212	0.48214	0.41339	0.56875
4.5	47.9684	0.71696	0.72549	0.75096	0.48214	0.41875	0.56875
4.75	48.1331	0.71696	0.72549	0.72981	0.48214	0.42768	0.57232
5	48.29777	0.71607	0.72549	0.68173	0.48304	0.42946	0.57321
5.25	48.4624	0.71429	0.72549	0.64519	0.48214	0.43393	0.57411
5.5	48.627	0.7125	0.72549	0.61442	0.48304	0.43839	0.57679
5.75	48.79155	0.70536	0.72647	0.56923	0.48393	0.44107	0.57857
6	48.95607	0.69732	0.72451	0.51923	0.48304	0.44464	0.57857
6.25	49.12054	0.69554	0.7049	0.47981	0.48661	0.44554	0.58036
6.5	49.28497	0.68393	0.68627	0.4375	0.48929	0.44643	0.58214
6.75	49.44935	0.67857	0.68529	0.40385	0.49464	0.44643	0.58571
7	49.61369	0.66607	0.65196	0.35096	0.49911	0.44732	0.58304
7.25	49.77797	0.66071	0.63725	0.32692	0.5	0.45	0.58304
7.5	49.9422	0.64464	0.60784	0.29615	0.50089	0.45268	0.58304
7.75	50.10638	0.63839	0.60588	0.26923	0.50179	0.45625	0.58214
8	50.2705	0.625	0.56961	0.22308	0.50625	0.46161	0.58661
8.25	50.43457	0.60893	0.55	0.19423	0.51429	0.46429	0.58839
8.5	50.59858	0.58929	0.52941	0.17596	0.51518	0.46607	0.58839
8.75	50.76252	0.57768	0.50392	0.15385	0.51786	0.46875	0.58929
9	50.92641	0.56607	0.48333	0.13365	0.51875	0.47143	0.58929
9.25	51.09022	0.55357	0.45196	0.11538	0.51875	0.47321	0.58929
9.5	51.25398	0.53839	0.44706	0.1	0.51875	0.47679	0.58929
9.75	51.41766	0.51875	0.42647	0.09375	0.51875	0.47946	0.58929
10	51.58127	0.5	0.40882	0.07913	0.525	0.48125	0.59018
10.25	51.74481	0.48214	0.37843	0.07644	0.525	0.48214	0.58929
10.5	51.90828	0.475	0.37157	0.06404	0.52321	0.48214	0.59018
10.75	52.07167	0.4625	0.33824	0.0574	0.52768	0.48214	0.58929
11	52.23499	0.44732	0.32353	0.04856	0.53125	0.48304	0.59018
11.25	52.39822	0.43125	0.29706	0.04067	0.53304	0.48393	0.59375
11.5	52.56138	0.41071	0.27451	0.03856	0.53304	0.48571	0.59196
11.75	52.72445	0.40268	0.26471	0.03837	0.53304	0.48839	0.59018
12	52.88743	0.39196	0.24216	0.03683	0.53214	0.49286	0.59286

12.25	53.05033	0.375	0.23431	0.03375	0.53304	0.49464	0.59643
12.5	53.21314	0.3625	0.21961	0.02885	0.53304	0.49732	0.59821
12.75	53.37586	0.34911	0.20392	0.02596	0.53304	0.49911	0.60357
13	53.53849	0.33929	0.1951	0.02163	0.53304	0.50089	0.60446
13.25	53.70102	0.32857	0.17941	0.02067	0.53304	0.50268	0.60446
13.5	53.86345	0.31964	0.17059	0.02	0.53393	0.50357	0.60625
13.75	54.02579	0.30536	0.15686	0.01962	0.53482	0.50536	0.60893
14	54.18803	0.29911	0.15098	0.01952	0.53571	0.51071	0.6125
14.25	54.35016	0.28482	0.13627	0.01952	0.53571	0.51339	0.61429
14.5	54.51219	0.26696	0.11961	0.01952	0.53571	0.51696	0.61429
14.75	54.67412	0.26786	0.11667	0.01971	0.53661	0.51696	0.61429
15	54.83594	0.25	0.10196	0.02029	0.53839	0.51786	0.61429
15.25	54.99764	0.23393	0.09804	0.02077	0.53839	0.51786	0.61875
15.5	55.15924	0.22768	0.09392	0.02135	0.53839	0.51786	0.62321
15.75	55.32072	0.21518	0.08608	0.02231	0.53839	0.51875	0.62321
16	55.48208	0.20893	0.07882	0.02385	0.53839	0.51964	0.62321
16.25	55.64333	0.19732	0.07824	0.02683	0.54018	0.52054	0.62321
16.5	55.80446	0.19018	0.07431	0.02798	0.54107	0.52232	0.625
16.75	55.96546	0.17946	0.06912	0.03077	0.54107	0.52768	0.62589
17	56.12635	0.17768	0.05941	0.03346	0.54286	0.52857	0.62589
17.25	56.2871	0.16607	0.05686	0.03606	0.54821	0.53125	0.62857
17.5	56.44773	0.15804	0.05059	0.03702	0.54911	0.53304	0.63125
17.75	56.60823	0.14821	0.04363	0.0375	0.54911	0.53393	0.63125
18	56.7686	0.14286	0.04039	0.03827	0.55	0.53482	0.63125
18.25	56.92883	0.13929	0.03941	0.03846	0.55089	0.53571	0.63214
18.5	57.08893	0.12768	0.03912	0.03856	0.55179	0.5375	0.63482
18.75	57.24889	0.12411	0.03892	0.03865	0.55268	0.53661	0.63482
19	57.4087	0.12232	0.03784	0.03913	0.55357	0.53661	0.63661
19.25	57.56838	0.11429	0.03588	0.0399	0.55357	0.53661	0.6375
19.5	57.72792	0.10804	0.03284	0.04115	0.55357	0.54196	0.63929
19.75	57.8873	0.10714	0.02971	0.04375	0.55357	0.54196	0.64286
20	58.04654	0.10179	0.02657	0.04635	0.55357	0.54643	0.64196
20.25	58.20563	0.09732	0.0251	0.04952	0.55357	0.54732	0.64018
20.5	58.36457	0.09107	0.02304	0.0525	0.55357	0.55	0.64107
20.75	58.52335	0.08929	0.02176	0.05413	0.55446	0.55089	0.64286
21	58.68197	0.08759	0.02078	0.05615	0.55982	0.55089	0.64464
21.25	58.84044	0.08152	0.0202	0.05702	0.5625	0.55268	0.64643
21.5	58.99874	0.07687	0.02	0.0576	0.5625	0.55268	0.64464
21.75	59.15689	0.07464	0.01961	0.05827	0.56607	0.55357	0.64375

22	59.31486	0.07625	0.01902	0.05952	0.56964	0.55357	0.65
22.25	59.47267	0.06107	0.01882	0.06096	0.57143	0.55357	0.65179
22.5	59.63031	0.05679	0.01853	0.06288	0.57143	0.55357	0.64821
22.75	59.78778	0.05429	0.01843	0.06577	0.57143	0.55357	0.64911
23	59.94508	0.05277	0.01814	0.06875	0.57232	0.55357	0.65446
23.25	60.1022	0.05062	0.01804	0.07183	0.57411	0.55357	0.65625
23.5	60.25914	0.04598	0.01794	0.07394	0.57589	0.55357	0.65982
23.75	60.4159	0.04304	0.01775	0.07577	0.57768	0.55446	0.66071
24	60.57247	0.03902	0.01804	0.07644	0.57946	0.55625	0.66071
24.25	60.72887	0.03759	0.01824	0.07673	0.58304	0.55714	0.66071
24.5	60.88507	0.03634	0.01824	0.07692	0.58482	0.55714	0.66071
24.75	61.04109	0.03589	0.01824	0.07702	0.58482	0.5625	0.66071
25	61.19691	0.0358	0.01843	0.07721	0.58571	0.56518	0.66071
25.25	61.35254	0.03571	0.01873	0.07788	0.58393	0.56875	0.66071
25.5	61.50798	0.03563	0.01892	0.07894	0.58661	0.56964	0.66071
25.75	61.66321	0.03554	0.01922	0.08029	0.58839	0.57054	0.66161
26	61.81825	0.03527	0.01931	0.08288	0.58839	0.57054	0.66071
26.25	61.97308	0.03491	0.0198	0.08394	0.58929	0.57054	0.66071
26.5	62.12771	0.03464	0.0199	0.08702	0.58929	0.57054	0.66071
26.75	62.28213	0.03393	0.0202	0.08933	0.58929	0.57143	0.66071
27	62.43634	0.03348	0.02069	0.09173	0.58929	0.57321	0.66161
27.25	62.59033	0.03268	0.02118	0.09308	0.58929	0.57946	0.66161
27.5	62.74411	0.03214	0.02167	0.09394	0.58929	0.58214	0.66161
27.75	62.89768	0.03143	0.02235	0.09452	0.58929	0.58571	0.66161
28	63.05102	0.03107	0.02324	0.09558	0.58929	0.58661	0.6625
28.25	63.20415	0.03071	0.02441	0.09587	0.58929	0.58929	0.6625
28.5	63.35704	0.03054	0.02608	0.09596	0.58929	0.58929	0.6625
28.75	63.50972	0.03071	0.02814	0.09615	0.58929	0.58929	0.66429
29	63.66216	0.03098	0.02961	0.09615	0.58929	0.58929	0.66518
29.25	63.81437	0.03125	0.03196	0.09615	0.58929	0.58929	0.66607
29.5	63.96635	0.0317	0.03353	0.09712	0.59018	0.58929	0.66696
29.75	64.11809	0.03188	0.03471	0.09904	0.59196	0.58929	0.66875
30	64.26959	0.03196	0.03578	0.10096	0.59286	0.58929	0.66964
30.25	64.42085	0.03214	0.03676	0.10192	0.59286	0.59018	0.67054
30.5	64.57186	0.03277	0.03765	0.10385	0.59464	0.59107	0.67232
30.75	64.72263	0.03304	0.03824	0.10577	0.59732	0.59196	0.67232
31	64.87315	0.03348	0.03873	0.10865	0.59732	0.59196	0.67232
31.25	65.02342	0.03393	0.03902	0.11058	0.59732	0.59375	0.675
31.5	65.17344	0.03438	0.03922	0.11154	0.59464	0.59643	0.67589

31.75	65.32319	0.03464	0.03922	0.11346	0.59107	0.59821	0.67589
32	65.47269	0.03509	0.03931	0.11442	0.59107	0.60357	0.67589
32.25	65.62193	0.03536	0.03941	0.11442	0.59107	0.60625	0.67768
32.5	65.7709	0.03545	0.03971	0.11442	0.58929	0.60357	0.67768
32.75	65.91961	0.03571	0.04	0.11442	0.59107	0.60446	0.67768
33	66.06804	0.0358	0.04078	0.11442	0.59018	0.60536	0.67857
33.25	66.2162	0.0358	0.04196	0.11442	0.58929	0.60625	0.67857
33.5	66.36409	0.03589	0.04353	0.11442	0.58929	0.60625	0.67857
33.75	66.5117	0.03598	0.04529	0.11442	0.58929	0.60625	0.67857
34	66.65903	0.03616	0.04824	0.11442	0.58929	0.60625	0.67946
34.25	66.80608	0.03661	0.04971	0.11442	0.58929	0.60625	0.67946
34.5	66.95284	0.03687	0.05176	0.11442	0.58839	0.60714	0.67946
34.75	67.09931	0.03732	0.05343	0.11442	0.58929	0.60714	0.67946
35	67.24549	0.0383	0.05588	0.11442	0.58929	0.60714	0.68125
35.25	67.39138	0.03982	0.05706	0.11442	0.59018	0.60714	0.68214
35.5	67.53697	0.0417	0.05814	0.11538	0.59018	0.60714	0.68214
35.75	67.68226	0.04446	0.05873	0.11538	0.59018	0.60804	0.68214
36	67.82725	0.04661	0.05971	0.11538	0.58929	0.60804	0.68214
36.25	67.97194	0.04839	0.06049	0.11538	0.58929	0.60804	0.68214
36.5	68.11631	0.04938	0.06147	0.11635	0.58929	0.60982	0.68214
36.75	68.26038	0.05036	0.06314	0.11923	0.58929	0.60982	0.68304
37	68.40413	0.05223	0.06931	0.12596	0.58929	0.60982	0.68304
37.25	68.54757	0.05286	0.07108	0.13077	0.58839	0.60982	0.68393
37.5	68.69068	0.05357	0.07324	0.13365	0.5875	0.61071	0.68393
37.75	68.83348	0.05438	0.0748	0.13462	0.58929	0.61071	0.68393
38	68.97595	0.05545	0.07657	0.1375	0.5875	0.61071	0.68482
38.25	69.11809	0.05768	0.07735	0.14038	0.58661	0.6125	0.68571
38.5	69.2599	0.06	0.07784	0.14423	0.5875	0.61696	0.68571
38.75	69.40137	0.06375	0.07833	0.14904	0.5875	0.61964	0.68661
39	69.54251	0.06652	0.07843	0.15192	0.57768	0.62321	0.68661
39.25	69.68331	0.06821	0.07863	0.15288	0.57768	0.62321	0.68661
39.5	69.82377	0.06964	0.07882	0.15385	0.57768	0.62321	0.68661
39.75	69.96388	0.0708	0.07961	0.15385	0.57321	0.62321	0.6875
40	70.10365	0.07143	0.0802	0.15385	0.57321	0.62411	0.6875

Table A.4 Optical data for glass-slide/aluminum/ZnSe-chiral-STF structure (Set-up #2).

ZnSe chiral STF			
Polarization of incident light		p	
Thickness of chiral STF	3 periods	4 periods	5 periods
θ (deg)	R/U_{inc}	R/U_{inc}	R/U_{inc}
5	0.49327	0.52523	0.48611
6	0.49712	0.54019	0.48796
7	0.55	0.54206	0.48426
8	0.55769	0.54206	0.48148
9	0.59615	0.54299	0.48148
10	0.59615	0.54393	0.48333
11	0.59615	0.54486	0.48889
12	0.59712	0.54579	0.49815
13	0.59615	0.5514	0.49815
14	0.59615	0.55607	0.49907
15	0.59615	0.55981	0.49907
16	0.59615	0.55981	0.5
17	0.59615	0.55981	0.50093
18	0.59808	0.54673	0.50093
19	0.59808	0.54579	0.5
20	0.59712	0.55421	0.50185
21	0.59615	0.56355	0.51111
22	0.59038	0.57196	0.51296
23	0.59615	0.57944	0.52222
24	0.59615	0.58224	0.53611
25	0.59327	0.58037	0.53704
26	0.59615	0.58224	0.53704
27	0.57308	0.59533	0.54259
28	0.57596	0.60935	0.56574
29	0.55769	0.61682	0.575
30	0.55865	0.61776	0.58704
31	0.51731	0.63458	0.61019
32	0.54038	0.63551	0.61204

33	0.55673	0.64019	0.61389
34	0.53846	0.64019	0.62778
35	0.52596	0.64112	0.63148
36	0.51923	0.65234	0.63056
37	0.51731	0.65421	0.63148
38	0.51635	0.65327	0.63056
39	0.5125	0.65514	0.63148
40	0.52019	0.65514	0.63519
41	0.55481	0.65607	0.63796
42	0.63462	0.65421	0.64815
43	0.65288	0.61682	0.66481
44	0.70962	0.6514	0.7213
45	0.75385	0.66916	0.78981
46	0.80769	0.66355	0.67778
47	0.84808	0.65327	0.32037
48	0.84615	0.69159	0.46204
49	0.69135	0.70935	0.53611
50	0.24808	0.71028	0.56759
51	0.03837	0.65327	0.59167
52	0.07654	0.58131	0.61111
53	0.17308	0.62804	0.62315
54	0.23173	0.63645	0.63056
55	0.30288	0.65421	0.64722
56	0.36154	0.65514	0.65
57	0.37596	0.65888	0.65556
58	0.40577	0.67103	0.66574
59	0.42596	0.68318	0.68519
60	0.44231	0.69159	0.6963
61	0.45577	0.6215	0.68519
62	0.47115	0.52243	0.70185
63	0.48077	0.57383	0.725
64	0.48365	0.5785	0.73704
65	0.49231	0.54299	0.68426
66	0.49904	0.5785	0.43148
67	0.50288	0.57944	0.2
68	0.50385	0.57944	0.20833
69	0.5125	0.57944	0.25926

70	0.51635	0.58037	0.31389
71	0.51827		0.33704
72	0.51923		0.36019
73	0.52212		0.37593
74	0.53365		0.40556
75	0.53365		0.41019